



Prediction of concrete materials compressive strength using surrogate models

Wael Emad^a, Ahmed Salih Mohammed^{b,c}, Rawaz Kurda^{d,e,f}, Kawan Ghafor^b, Liborio Cavalieri^g, Shaker M.A.Qaidi^{e,h}, A.M.T. Hassanⁱ, Panagiotis G. Asteris^{j,*}

^a Department of Civil Engineering, Komar University, Iraq

^b Civil Engineering Department, College of Engineering, University of Sulaimani, Iraq

^c Civil Engineering Department, American University of Iraq, Sulaimani, Iraq

^d Department of Highway and Bridge Engineering, Technical Engineering College, Erbil Polytechnic University, Erbil 44001, Iraq

^e Department of Civil Engineering, College of Engineering, Nawroz University, Duhok 42001, Iraq

^f CERIS, Civil Engineering Architecture and Georesources Department, Instituto Superior Técnico, Universidade de Lisboa, Av. Rovisco Pais, 1049-001 Lisbon, Portugal

^g Department of Civil, Environmental, Aerospace and Materials Engineering, University of Palermo, Palermo, Italy

^h Department of Civil Engineering, College of Engineering, University of Duhok, Duhok, Kurdistan-Region, Iraq

ⁱ American University of Iraq, Sulaimani (AUIS), Sulaimani, Kurdistan Region

^j Computational Mechanics Laboratory, School of Pedagogical and Technological Education, Heraklion, 14121 Athens, Greece

ARTICLE INFO

Keywords:

Artificial neural networks
UHPFRC
Compressive strength
Concrete materials
Silica fume
Fiber aspect ratio
Soft computing

ABSTRACT

Using soft computing methods could be of great interest in predicting the compressive strength of Ultra-High-Performance Fibre Reinforced Concrete (UHPFRC). Therefore, this study developed four soft computing techniques. The models are the Linear- relationship (LR), pure quadratic, M5P-tree (M5P), and artificial neural network (ANN). The models were trained and developed using 306 datasets comprising 11 input parameters, including the curing temperature (T), the water-to-cement ratio (w/c), silica fume (SF), cement content (C), fiber content (Fb), water (W), sand content (S), superplasticizer (SP), fiber aspect ratio (AR) and curing time (t). Experimental results were used and compared to the model performances to validate the developed models. The models were developed based on 192 training datasets, and the model's accuracy was checked using 41 testing datasets; the model's outcomes were validated using 32 experimental datasets. The results show a high prediction accuracy of the compressive strength of UHPFRC using ANN models. Based on the optimum developed ANN model, a closed-form equation is presented, proving to be a reliable and useful tool for researchers and, above all, for practicing engineers in compressive strength prediction.

1. Introduction

In the construction industry, ultra-high performance fiber reinforced concrete (UHPFRC) is increasingly used, in particular, to construct blast-resistant high-rise structures, as it provides a very high compressive and tensile strength [1]. This new type of concrete has a higher cement content than standard concrete, as well as a higher fiber content, fine sand with particle sizes less than 1 mm, water/cement ratio ranging between 0.16 and 0.23, superplasticizer, high ratio of fiber aspect ratio (the diameter and the length were 0.2 mm and 12 mm respectively) [2–6]. Concrete packing is densified by replacing cement with

pozzolanic materials or mineral admixtures such as; Silica fume (SF), Nano silica, Pulverized fly ash, and Metakaolin [7–11]. The sand particle size is critical in reducing the cost of producing UHPFRC samples. The impact of replacing silica sand with two natural grains of sand and Recycled Glass Cullet (RGC) was investigated by Yang et al. [5]. The results showed that the flowability of the mixture was reduced with the inclusion of angular particles. The natural sand particle types were found to be suitable as silica sand replacements without affecting the ductility behaviour and mechanical properties of UHPFRC, but the inclusion of RGC decreased the flexural and compressive strengths by up to 15 %. Most of the research has focused on preparing UHPFRC at an elevated temperature as it provides increased strength for a short curing

* Corresponding author.

E-mail addresses: wael.mahmood@komar.edu.iq (W. Emad), ahmed.mohammed@univsul.edu.iq (A. Salih Mohammed), Rawaz.Kurda@tecnico.ulisboa.pt (R. Kurda), kawan.ghafor@univsul.edu.iq (K. Ghafor), liborio.cavalieri@unipa.it (L. Cavalieri), shaker.abdal@uod.ac (S. M.A.Qaidi), aram.hassan@auis.edu.krd (A.M.T. Hassan), asteris@aspete.gr (P.G. Asteris).

Nomenclature

ANN(s)	Artificial Neural Network(s)
LR	Linear Relationship model
M5P	M5P-tree model
UHPFRC.	Ultra-high-performance fiber-reinforced concrete
w/c	Water to cement ratio
C	Cement content
f'_c	Concrete compressive strength
SF.	Silica fume
SP.	Superplasticizer
AR	Steel fiber aspect ratio
F	The content of fiber, (kg/m^3)
T	Curing temperature
t	Curing time
FC	Fiber content, (%)
W	Water content
S	Sand content
R ²	The coefficient of determination
RMSE	Root Mean Square Error
MAE	Mean Absolute Error

duration; however, such a curing method increases the cost of UHPFRC, and it is an application. Yang et al. [5] reported that concrete samples cured at 90 °C for 7 days attained 80, 90, and 90 % higher compressive and flexural strengths than samples cured for the same duration at 20°C.

Hassan et al. [12] studied the mechanical properties of UHPFRC and found that the curing temperature substantially impacts the specimen's strength. Cube and beam specimens were cast and cured for up to a year at temperatures 10, 20, 30, and 90 °C. The three lower curing temperatures were chosen to simulate conditions for UHPFRC cast-in-situ applications, and the findings were compared to those of the 900C curing temperature specimens. At 28 days, the 20 and 30 °C specimens matched the 90 °C samples in compressive and flexural strengths, whereas the 10 °C specimens matched the 90 °C samples at 90 days of curing.

Magureanu et al. [13] used two distinct curing regimes for 5 days, water curing at 20 °C and thermal curing at 90 °C. After testing all specimens at 6 days, they found that compressive and flexural strength increased to 181 and 17.5 MPa, respectively. The identical samples cured in water at 20 °C had compressive and tensile strengths of 130 and 6 MPa, respectively.

Karim et al. [14] studied how fiber concentration and length affected UHPFRC compressive strength. With 2.2 % of micro steel fibers replacing 25 % of the total fiber with long fibers, the compressive strength increased by 6.5 %. Kang et al. [15] found that fiber content linearly affects flexural strength. On the other hand, Kwon et al. [16] produced a new UHPFRC to determine the best fiber volume fraction at a reduced cost. The results showed that the mechanical properties improved significantly when the fiber volume content ranged between 2.5 and 3 %. Wu et al. [17] used varied fiber shapes and volume contents (0–3 %) to test the compressive and flexural strength of UHPFRC. Adding 3 % straight, corrugated, or hooked-end steel fibers lowered concrete mix flowability by 41, 44, and 51 %. Hooked-end specimens had the highest compressive and flexural strength increases (171 and 42 MPa), and straight fiber specimens had the lowest (43 %). Abbas et al. [18] studied the influence of steel fiber length (8, 12, and 16 mm) and fiber content (1, 3, and 6 % by volume) on UHPFRC mechanical characteristics. UHPFRC mechanical characteristics improved as fiber content increased.

Nguyen et al. [19] evaluated the tensile stress-strain behavior of UHPFRC using parameters such as gauge length, sample size, and geometry, including the same microfiber content (smooth and twisted steel fiber). They showed that the relationship between concrete toughness and gauge length is complicated.

Yoo et al. [20] studied the impact of two major parameters on the compressive strength of UHPFRC, using different placing methods (center and corner placing) and fiber lengths (varied between 13 and 30 mm). The results showed that the first crack strength is not significantly affected by the fiber length and that the compressive strength increases when the fiber length is shorter than 19.5 mm. The placing method adversely affected the flexural strength in both the first and ultimate cracking load. A higher strength was obtained for concrete placed in the center. Yang et al. [6] suggested that the placing method also affects the

Table 1
Summary of different UHPFRC mixtures with silica fume.

Ref.	w/c (%)	C (kg/m^3)	W (kg/m^3)	S (kg/m^3)	SP (kg/m^3)	SF (kg/m^3)	t (day)	F (kg/m^3)	Fiber AR	T (°C)	f'_c (MPa)
[2]	0.3	657	185	1051	40	119	7–180	157	65	10–90	101.6–168
[4]	0.25	1092–1280	273–320	292–647	30.2–77.2	273–320	28	0–468	63.50	60	124–162
[5]	0.18	657	116.46	1050	1.05	119.4	7–56	156	65	20, 90	120–177
[11]	0.24–0.32	960	227–306	960	24	240	7, 28	192	72	20	100–147
[14]	0.25	1500	372	650	40	175	7–28	0–188	60, 120	28	93–118
[17]	0.22	784–809	171–177	1045–1079	20.9–21.6	261–270	3–90	0–234	65.00	20	93–166
[21]	0.26	700	180	1104	30	50	28	0–78	65	20	105–138
[22]	0.15	712	109	1020	30.7	231	3–56	156	62.5	60, 90	139–186
[23]	0.2	850	170	850	76.5	226	28	78–157	65	20	145–150
[24]	0.28	657	185	1051	40	119	7–28	157	65	90	145–150
[25]	0.23–0.33	612–874	202.1	1273.4	45.9	43.7	7, 28	39–195	65	21	99–156
[26]	0.21	1050	224	678	42	350	5	0–117	60	80	107–140
[27]	0.18	800	144	1250	80	240	7, 28	40	16.25	25	120–149
[28]	0.35	413	143	1593–1827	9.75	32.5	28	0–234	50	20	114–128
[29]	0.14–0.16	998.8	141–164.5	898–1014	49.4–88.2	176.25	7–28	0–78	722	21	112–160
[30]	0.2	1163–1543	233–313	607–1923	34.1–89.7	5.5–20	28	0–468	0–63.5	60, 90	131–169
[31]	0.20	788	157.60	795.88	14.77	197	28	157	81	200	140–171
[32]	0.35–0.36	641–648	228	943–952	34.2–45.6	40–41	28	312–390	65	23	146–150
[33]	0.22	788	173	867	14.77	197	28	0	0	20	132
[34]	0.19	720	136.00	1025	30.00	240	28	0–157	63.50	22	112–149
[35]	0.22	800	176.00	896–1056	39.00	200	28	80–240	59.00	21	150–152
[36]	0.25	900	225.00	826	36.00	225	56	0–156	60.00	25, 200	145–184
[37]	0.18	900	162	764–1055	40	44–220	28	157	85	22	125–161
[38]	0.16–9.22	703–950	155.00	690	24.5–28.5	285	28	0–117	0–1014	21, 125	101–178
[39]	0.24	900	216	1125	27	180–270	7, 28	0–154.8	380.79	2	90–136.6
Current study	0.28	657	185	1051	40	119	7–180	157	65	10–90	97.7–173.5
Ranged between	0.14–0.36	413–1543	109–372.5	292–1923	1.05–89.7	5.5–350	3–180	0–468	0–1014.29	10–200	90.18–186

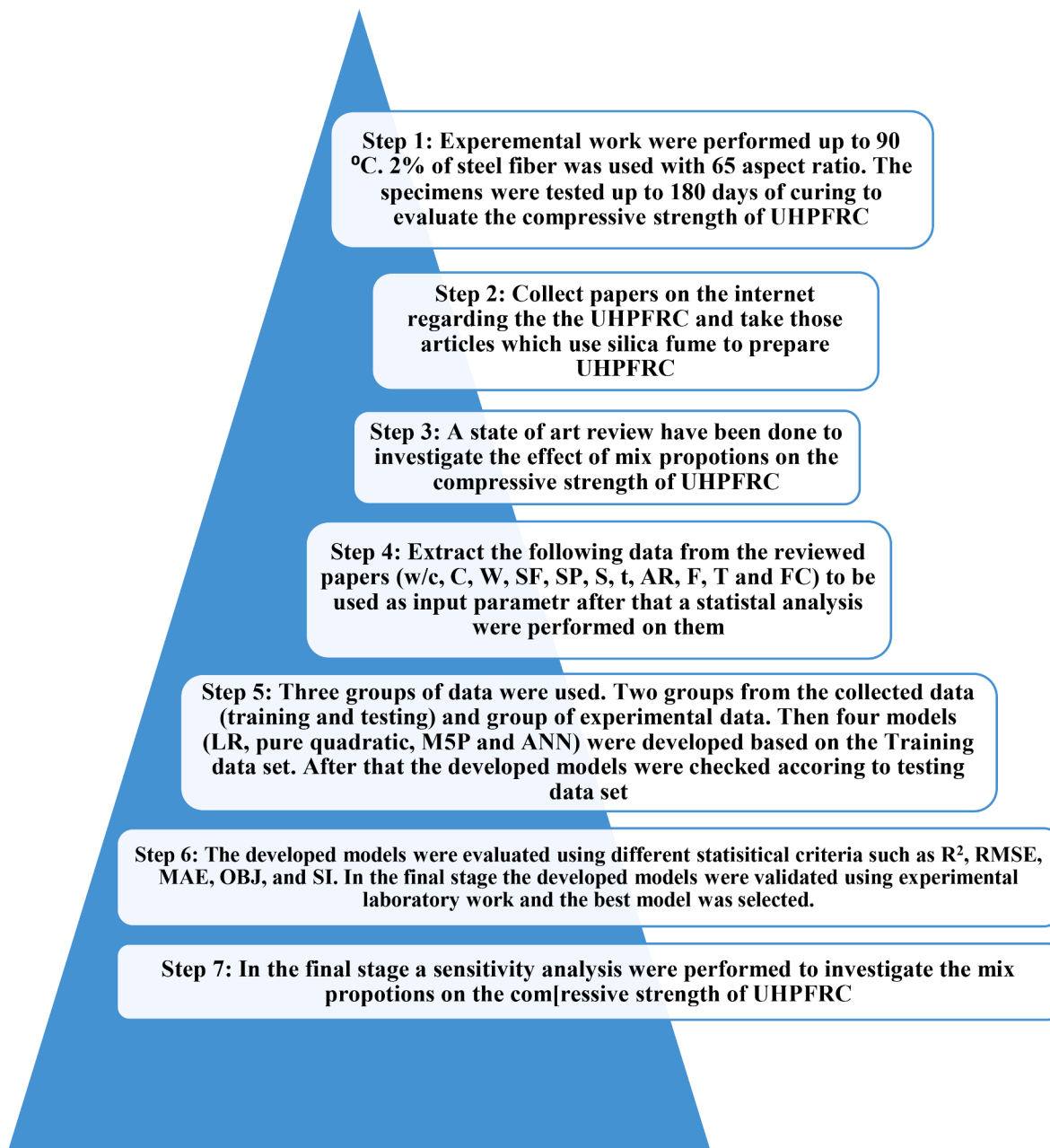


Fig. 1. The pyramid diagram for the current study's procedure.

fiber orientation and arrangement inside the matrix. An optimized method used a higher flexural strength to cast the mixture [21]. Few relationships have been presented for predicting the compressive strength, Young Modulus, and crack mouth opening (CMO) of UHPFRC (fresh and hardened) [4,22].

This research aims to assess the impact of different mixture compositions on the compressive strength of UHPFRC. To this end, various modeling techniques such as linear, pure quadratic, M5P-tree, and ANN were developed using 274 data samples compiled from previous research studies and 32 experimental laboratory data. The main objectives are: (i) to conduct statistical analysis and assess the impact of different mixture compositions on the compressive strength of UHPFRC and (ii) to develop a reliable model (linear, pure quadratic, M5P-tree, and ANN models) for the prediction of the compressive strength of UHPFRC using various prediction accuracy performance indexes; iii) to determine the most reliable model for assessing the compressive strength of UHPFRC.

This paper is organized into the following sections based on the above. [Section 2](#) is devoted to the methodology followed in the proposed research. [Section 3](#) presents the statistical assessment of the mix proportions. Experimental work procedures were presented in section 4. [Sections 5–7](#) are devoted to the models and assessment criteria for the developed models and analysis.

2. Methodology

Different curing temperatures were tested to show how they affected UHPFRC compressive strength. The experiment result was compared to data gathered from previous studies. The training datasets comprised two-thirds of the total datasets and were used to develop the models. The other group with one- to three of the data set was used to test the experimental data to validate the developed models. [Table 1](#) presents the various input parameter used for the prediction of the compressive strength of UHPFRC including (a) SF content, (b) cement content, (c) w/



Fig. 2. Specimen preparation and curing.

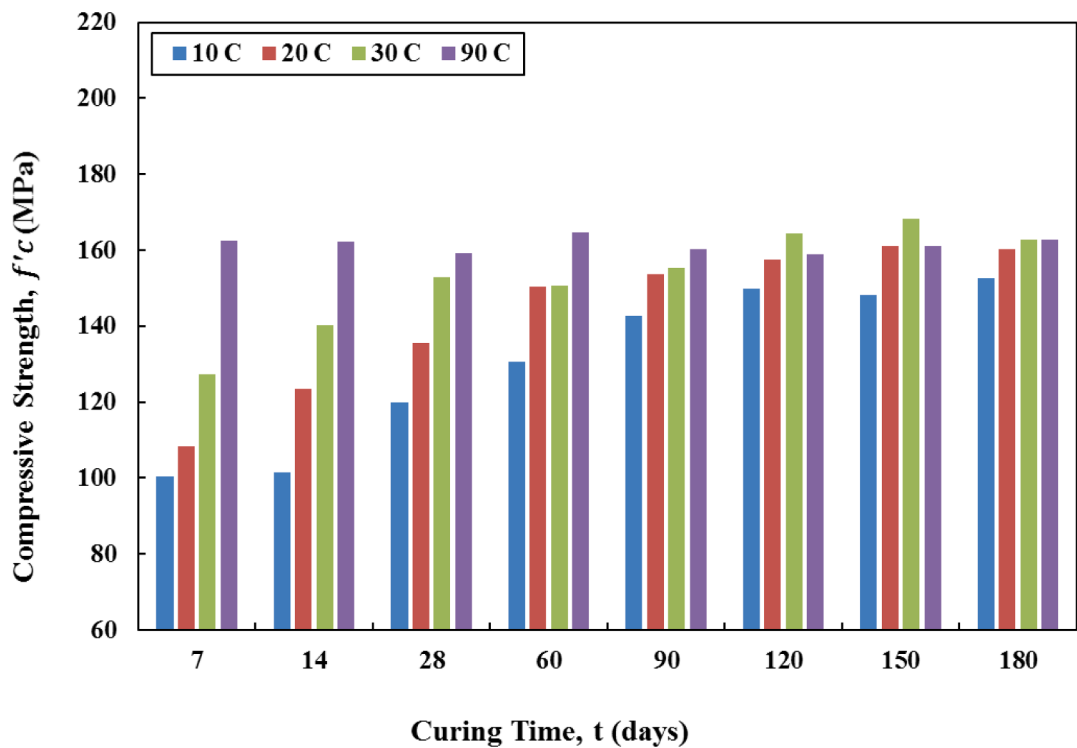


Fig. 3. Variation of the compressive strength of UHPFRC tested at different curing times under different temperature.

c, (d) curing temperature, (e) SP content, (f) sand, (g) curing time, (h) fiber content, (i) fiber AR, (j) Water content, and (k) SP content. The main steps of the research methodology are shown in Fig. 1.

Step 1: Experimental work was performed for four curing temperatures 10, 20, 30, and 90 °C. 2 % of steel fiber was used with a 65 aspect ratio. The specimens were tested up to 180 days of curing to evaluate the compressive strength development of UHPFRC.

Step 2: Data was gathered from previous research studies.

Step 3: The input variables were subjected to statistical analysis.

Step 4: The data were randomly split into training, testing, and validation (Experimental laboratory) datasets.

Step 5: Four soft computing techniques were developed using the training datasets. The experimental data work was compared to the models' performance.

Step 6: Various prediction accuracy performance indexes were used to compare the developed models.

Step 7: Sensitivity analyses were performed to identify the input

parameter that most significantly affects the compressive strength of UHPFRC.

3. Experimental work

This study's mix proportions include 657 kg/m³ cement (CEM1: 52.5 N), 119 kg/m³ silica fume, and 1051 kg/m³ 0.27-mm silica sand. 40 kg/m³ superplasticizer, 157 kg/m³ steel fiber (2 % of the mix volume). First, the matrix's dry elements were weighed and mixed for 5 min. Then, superplasticizer water was applied. After 10 min of mixing, the material became a wet paste concrete with good flow and cohesion. Finally, 2 % of the composite volume was steel fibers. The 0.20 mm fibers were 13 mm long. 65-aspect-ratio steel fiber. The composite was stirred for 2 min to disperse the steel fibers. The specimens were cast in steel molds and vibrated for a minute. UHPFRC specimens for 10, 20, and 30 °C curing temperatures were wrapped in polythene 'cling film' and taped in their molds before submerging in water curing tanks. After



Fig. 4. Typical compressive failure shape for UHPFRC specimens.

casting, UHPFRC specimens for 90 °C curings were covered with moist hessian and polythene and cured at 20 °C for 1 day. The three lower curing specimens were demolded the next day and returned to their curing tanks until testing days. The 90 °C curing specimens were immersed in water for two days at 90 °C. The 90 °C samples were removed after 2 days and stored dry until testing. UHPFRC specimen f'_c developments were measured per BS EN 12390-3 (See Fig. 2).

3.1. Experimental results

Fig. 3 illustrates UHPFRC compressive strength development after 180 days at different temperatures. Time and curing temperature improve compressive strength. Strength development stopped at 7 days for 90 °C curing samples but continued for 30, 20, and 10 °C samples. The density of the cube samples was measured before starting the compression test. This UHPFRC mix's density was 2.337–2.477 g/cm³ regardless of curing. Low water and high fillers like silica fume contribute to the high density. **Fig. 4** shows a typical compressive failure shape for UHPFRC specimens. Data from prior studies were used to build empirical equations to predict UHPFRC compressive strength theoretically. The equations were confirmed using an experimental investigation at various curing temperatures.

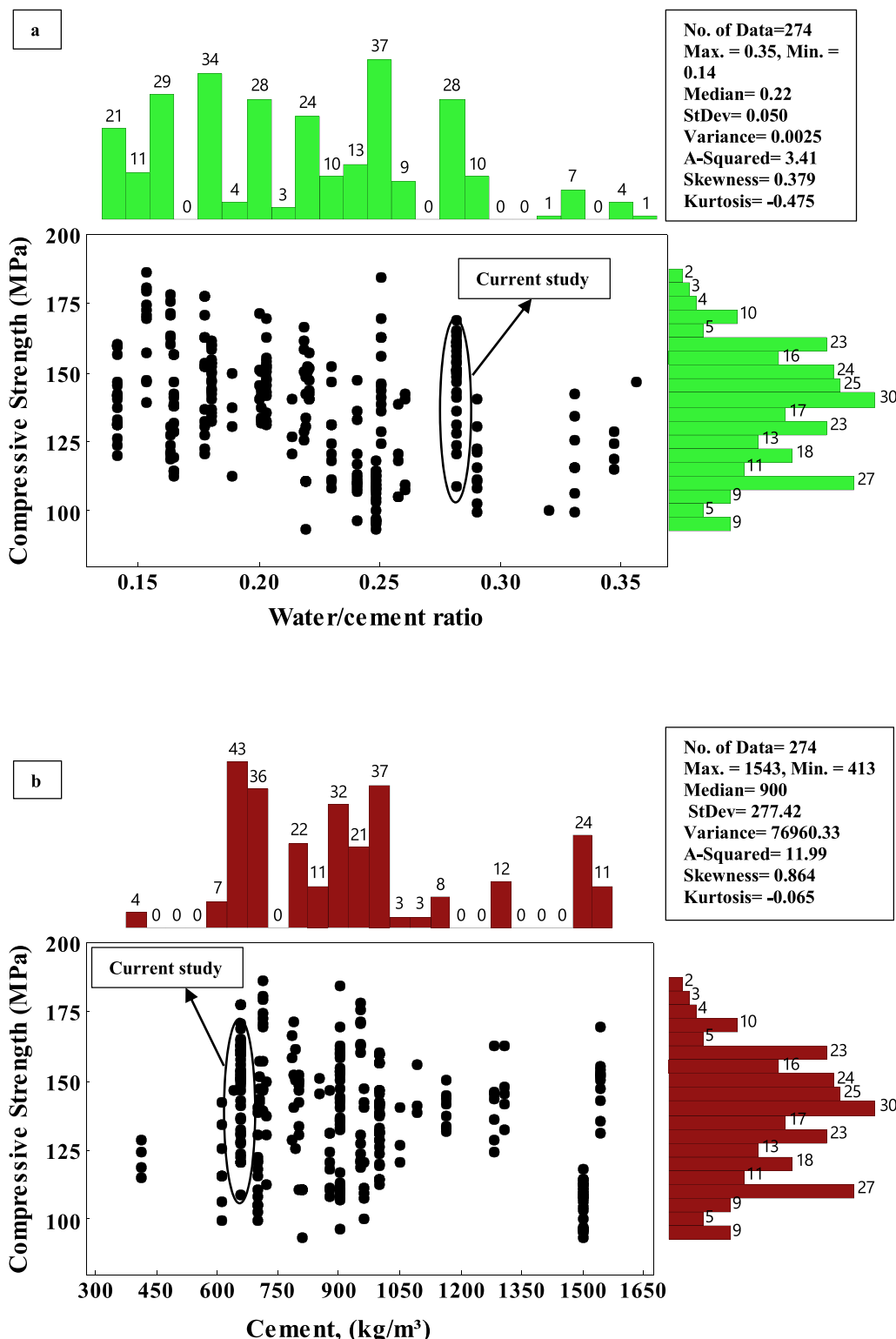
4. Statistical evaluation

Statistical analysis was conducted to determine which of the input parameters affects the compression strength of UHPFRC (**Table 2**). Thus, the plot of all considered parameters, including (a) SF content, (b)

Table 2

The statistical analysis of the collected datasets from the literature.

Data	Variable	Total count	Mean	Standard deviation	Variance	Coefficient of variation	minimum	maximum
Training dataset	w/c	192	0.220	0.051	0.00267	23.49	0.14	0.35
	C (kg/m ³)	192	932.4	278.3	77470.8	29.85	413	1543
	W (kg/m ³)	192	202.3	71.51	5113.42	35.35	109.00	372.5
	S (kg/m ³)	192	981.6	291.2	84810.1	29.67	292	1923
	SP (kg/m ³)	192	39.11	18.86	355.55	48.21	1.05	89.7
	SF (kg/m ³)	192	164.3	91.94	8452.45	55.94	5.5	350
	t (days)	192	30.35	29.54	872.51	97.33	4	180
	F (kg/m ³)	192	134.0	99.25	9851.13	74.05	0	468
	AR	192	195.5	257.9	66491.0	131.88	0	1014.3
	T (C°)	192	42.02	34.88	1216.81	83.02	10	200
	FC (%)	192	1.926	1.191	1.4197	61.85	0	6
	σ_c (MPa)	192	136.8	21.21	450.01	15.50	93.00	186
Testing dataset	w/c	41	0.21	0.05	0.0024	23.60	0.14	0.33
	C (kg/m ³)	41	953	305	93,365	32.05	612.4	1543
	W (kg/m ³)	41	200	80.5	6475.6	40.10	109.0	372.5
	S (kg/m ³)	41	954	206	42,638	21.64	607.0	1273.4
	SP (kg/m ³)	41	39.7	19.9	397.35	50.10	1.05	84.6
	SF (kg/m ³)	41	152	82.8	6852.2	54.36	20	285
	t (days)	41	26.6	25.1	632.02	94.22	3	120
	F (kg/m ³)	41	119	67.1	4503.4	56.21	0	312.0
	AR	41	229	263	69,654	115.02	60	772.6
	T (C°)	41	43.0	40.9	1672.8	94.95	100	200
	FC (%)	41	1.73	0.79	0.630	45.64	0	4
	σ_c (MPa)	41	133	19.9	398.75	14.97	100	184
Validation dataset (Experimental Data)	w/c	32	0.21	0.05	0.0027	24.03	0.14	0.34
	C (kg/m ³)	32	940	270	73167.5	28.76	413	1543
	W (kg/m ³)	32	203	72.2	5212.4	35.56	109	372.5
	S (kg/m ³)	32	975	265	70,359	27.19	310	1640
	SP (kg/m ³)	32	42.1	17.7	314.98	42.15	9.75	84.6
	SF (kg/m ³)	32	175	83.9	7040.5	47.87	5.5	320
	t (days)	32	28.7	26.4	697.31	91.99	7.00	150
	F (kg/m ³)	32	110	73.9	5459.0	66.62	0.0	312.0
	AR	32	186	251	63,469	134.95	0.0	722.2
	T (C°)	32	39.6	37.7	1421	95.06	20	200
	FC (%)	32	1.66	0.88	0.776	52.80	0	4
	σ_c (MPa)	32	136	20.7	429.82	15.21	95.8	178



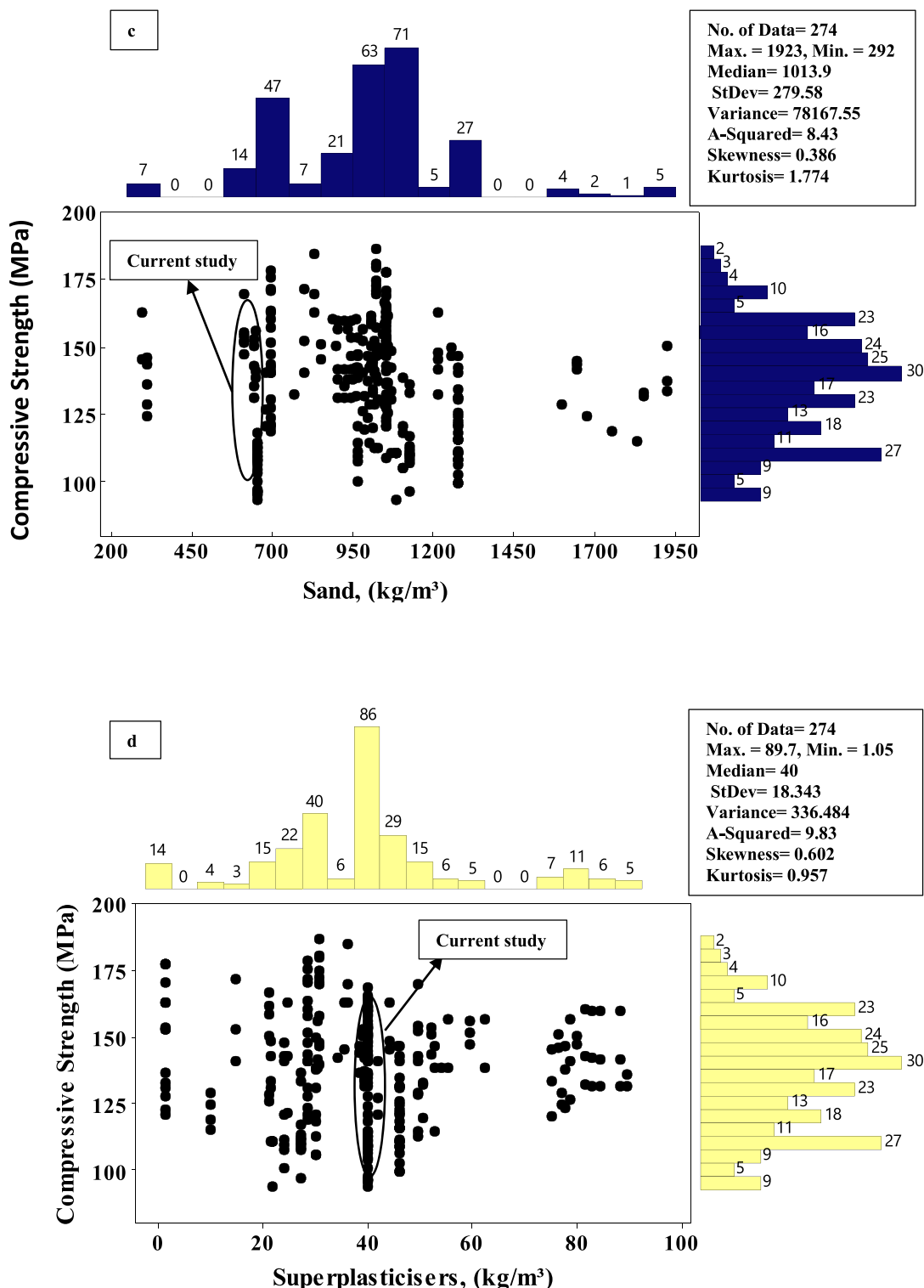


Fig. 5. (continued).

(a) shows the connection of f'_c with the w/c and the histogram of the w/c ratio.

(ii) Cement content.

According to the collected data, the cement content of UHPFRC

mixtures ranged between 413 and 1543 kg/m^3 and an average of 900 kg/m^3 . From the statistical analysis, the other variables' values were as follows: variance of 76960.33, A-squared of 11.99, the SD of 277.42, and skewness and kurtosis were 0.864 and – 0.065, respectively (Fig. 5(b)).

(iii) Sand content.

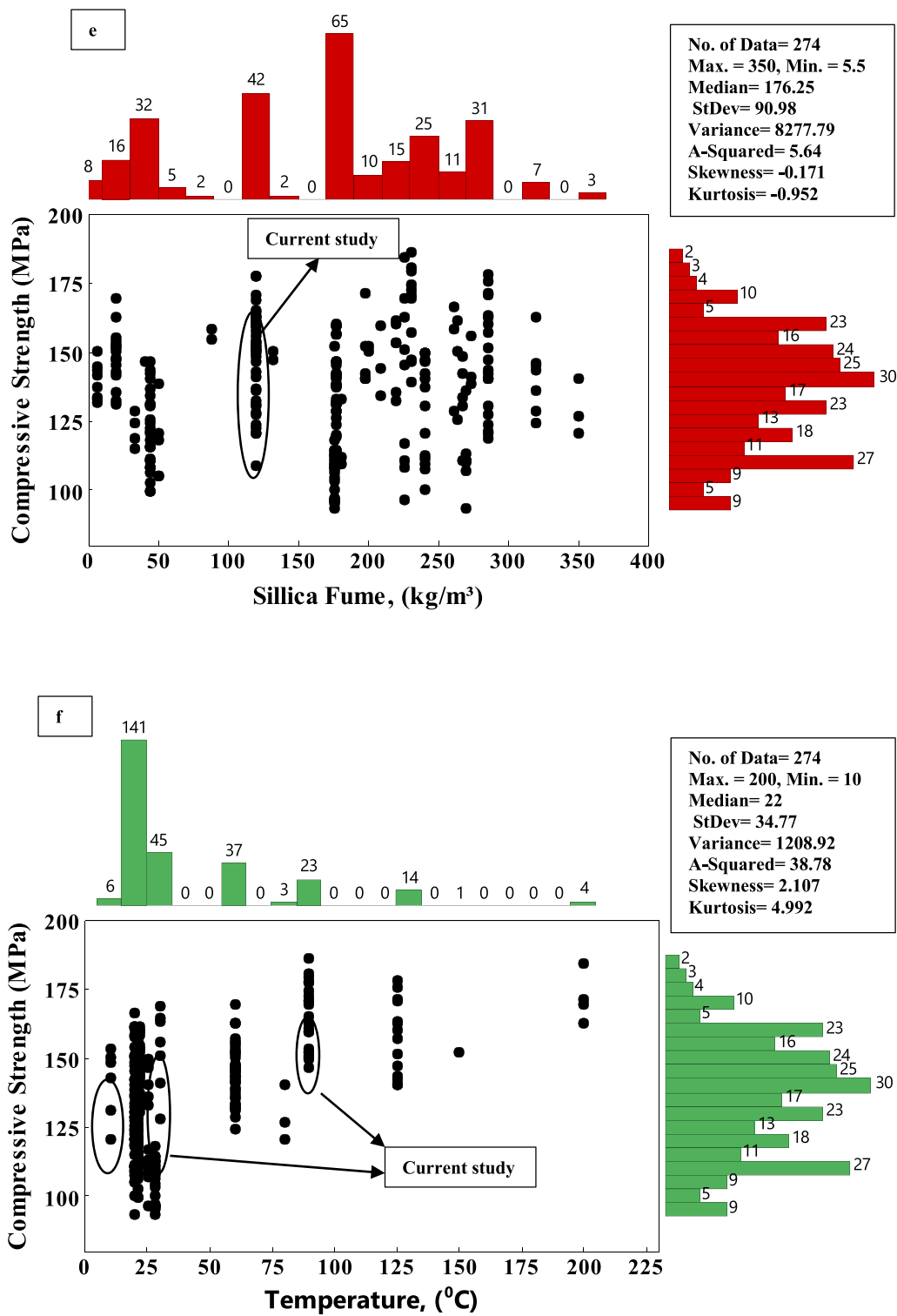


Fig. 5. (continued).

The size of the sand used for the UHPFRC mixtures was less than 20 mm, but more than 95 % of the data used a size of less than 8 mm. Different types of sand were used. As for sand content, the value ranged from 292 to 1923, with a median value of 1013.9 kg/m^3 . From the statistical analysis, the values for other variables were as follows: variance of 78167.55, A-squared of 8.43, a standard deviation of 279.58, and

value of skewness and kurtosis were 0.386 and 1.774, respectively, as shown in Fig. 5(c).

(iv) SP content.

Due to the very low amount of water in the UHPFRC mixes, the SP

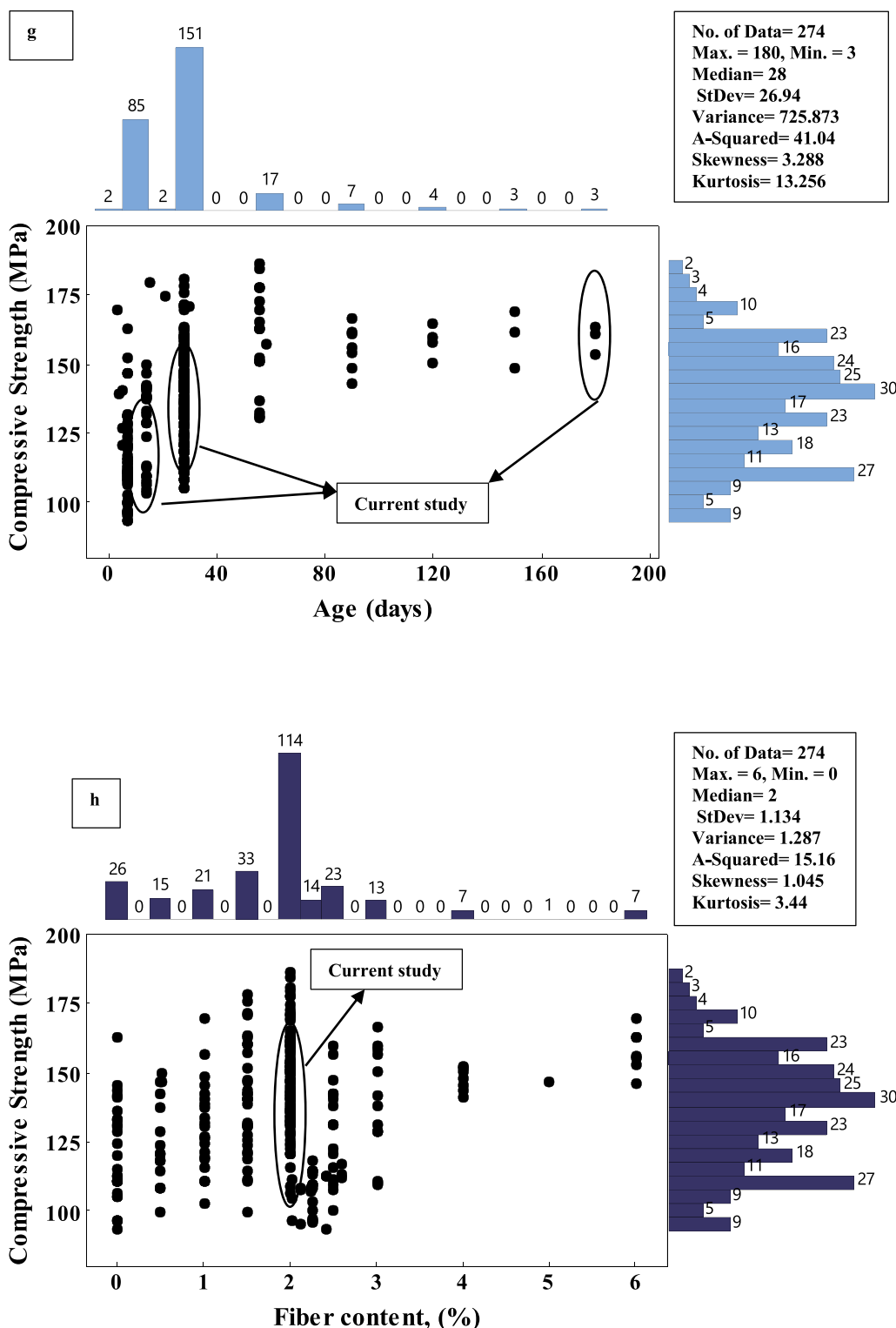


Fig. 5. (continued).

values ranged between 1.05 to 89.7 kg/m³ with a median of 40 kg/m³. From the statistical analysis, the values for other variables were as follows: variance of 336.484, A-squared of 9.83, a standard deviation of 18.343, and skewness and kurtosis were 0.602 and 0.957, respectively (Fig. 5(d)).

(v) SF content.

Based on the total collected data, the SF content of UHPFRC mixtures ranged between 5.5 and 350, with an average of 176.25 kg/m³. From the statistical analysis, the values for other variables were as follows: variance of 8277.79, A-squared of 5.64, the standard deviation of 90.98, and

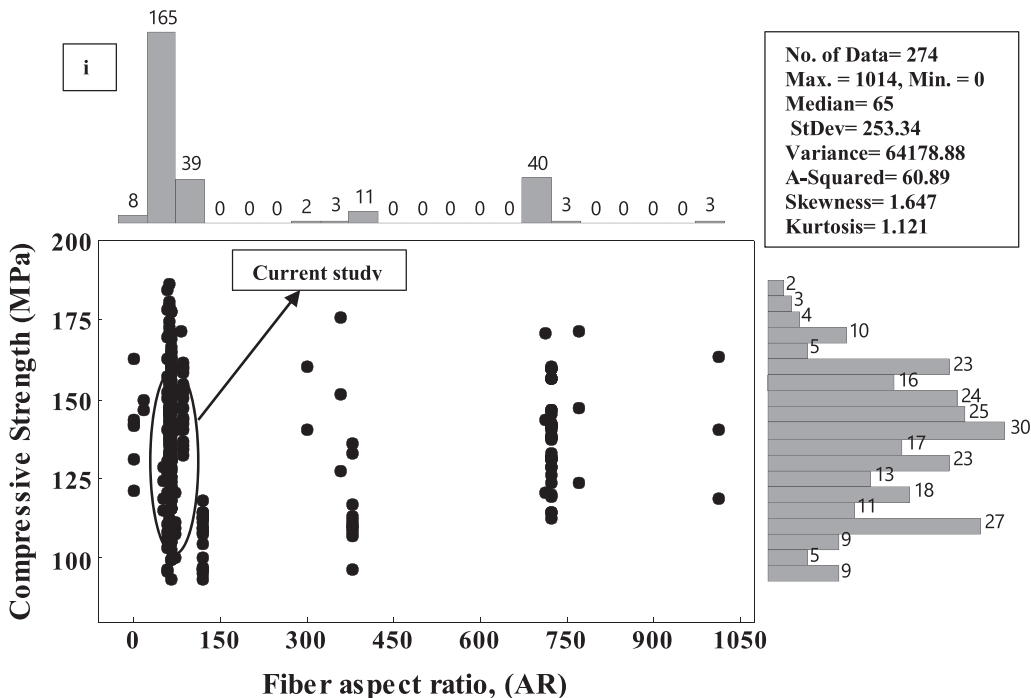


Fig. 5. (continued).

	w/c	C	W	S	SP	SF	t	F	AR	T	FC	σ_c
w/c	1.00	-0.18	0.41	0.17	-0.24	-0.30	0.21	0.27	-0.51	-0.12	0.10	-0.34
C	-0.18	1.00	0.81	-0.51	0.35	0.00	-0.28	0.22	0.07	-0.01	0.24	-0.25
W	0.41	0.81	1.00	-0.41	0.12	-0.10	-0.13	0.37	-0.28	-0.05	0.28	-0.43
S	0.17	-0.51	-0.41	1.00	-0.13	-0.55	0.06	-0.16	-0.13	-0.22	-0.24	-0.05
SP	-0.24	0.35	0.12	-0.13	1.00	-0.14	-0.13	-0.17	0.43	-0.23	-0.03	-0.01
SF	-0.30	0.00	-0.10	-0.55	-0.14	1.00	-0.10	-0.17	0.24	0.19	-0.07	0.08
t	0.21	-0.28	-0.13	0.06	-0.13	-0.10	1.00	0.11	-0.20	0.05	0.05	0.45
F	0.27	0.22	0.37	-0.16	-0.17	-0.17	0.11	1.00	-0.46	0.04	0.91	0.22
AR	-0.51	0.07	-0.28	-0.13	0.43	0.24	-0.20	-0.46	1.00	-0.07	-0.16	0.00
T	-0.12	-0.01	-0.05	-0.22	-0.23	0.19	0.05	0.04	-0.07	1.00	0.06	0.52
FC	0.10	0.24	0.28	-0.24	-0.03	-0.07	0.05	0.91	-0.16	0.06	1.00	0.26
σ_c	-0.34	-0.25	-0.43	-0.05	-0.01	0.08	0.45	0.22	0.00	0.52	0.26	1.00

Fig. 6. Correlation matrix for the properties of UHPFRC.

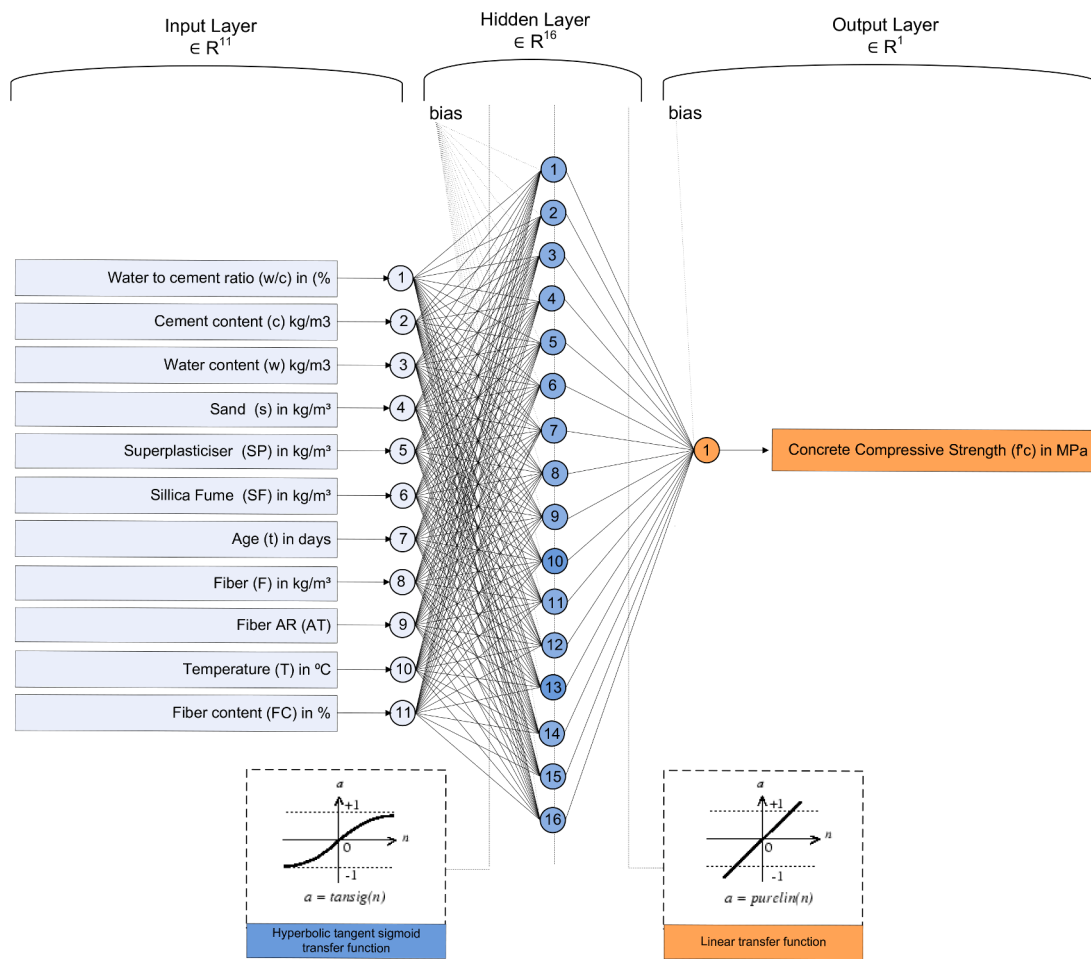


Fig. 7. Optimal neural network model structure.

the value of skewness and kurtosis were -0.171 and -0.952 , respectively. The f'_c and SF content connection with the normal distribution and histogram of SF content is reported in Fig. 5(e).

(vi) Curing temperature.

Different regimes are normally used for curing UHPFRC samples, such as normal water curing or thermal curing, especially in the first three days of curing. In the collected data, the curing temperature ranged between 10 and 200C° with a median of 22C° . From the statistical analysis, the values for other variables were: a variance of 1208.92 . Fig. 5 (f) shows the connection between f'_c and they are the curing temperature and the histogram of the curing temperature.

(vii) Curing time.

Extending the curing time for a sufficient period is important for the hydration process. The testing age ranged from 3 days to six months (180 days). From the statistical analysis, the values for other variables were as follows: variance of 725.873 , A-squared of 41.04 , and a standard deviation of 26.94 (Fig. 5 (g)).

(viii) Fiber content.

Fiber is the main parameter for designing UHPFRC and is the most expensive component responsible for improving the tensile strength three times more than normal strength concrete. The fiber content range ranged from 0 to 6% , with a median of 2% from the collected data. And from the statistical analysis, the values for other variables were as

follows: variance of 1.287 , A-squared of 15.16 , a standard deviation of 1.134 , and the value of skewness and kurtosis were 1.045 and 3.44 , respectively. The connection of f'_c with Fiber content, and the histogram of fiber content is exposed in Fig. 5(h).

(ix) Fiber aspect ratio.

The fiber length of UHPFRC mixtures ranged between 0 and 1014 , with a median of 65 . The variance, A-squared, and SD were 64178.88 , 60.89 , and 253.34 . The skewness and kurtosis values were 1.647 and -1.121 , respectively. The relationship between f'_c and fiber AR with the histogram of fiber AR is presented in Fig. 5(i).

(x) Stress at failure (Compression strength).

According to the total collected data, the f'_c of UHPFRC mixtures ranged between 90.18 and 186 N/mm^2 , with an average of 138.5 MPa . From the statistical analysis, the values of the other variables were as follows: variance of 435.37 , A-squared of 1.83 , a standard deviation of 20.87 , and value of skewness and kurtosis were -0.106 and -0.745 , respectively.

5. Modeling

According to the correlation matrix, no direct relationship was obtained from the analyzed data results in section 3 (Fig. 6). Therefore, various soft computing models for predicting UHPFRC were trained and developed (See Fig. 7).

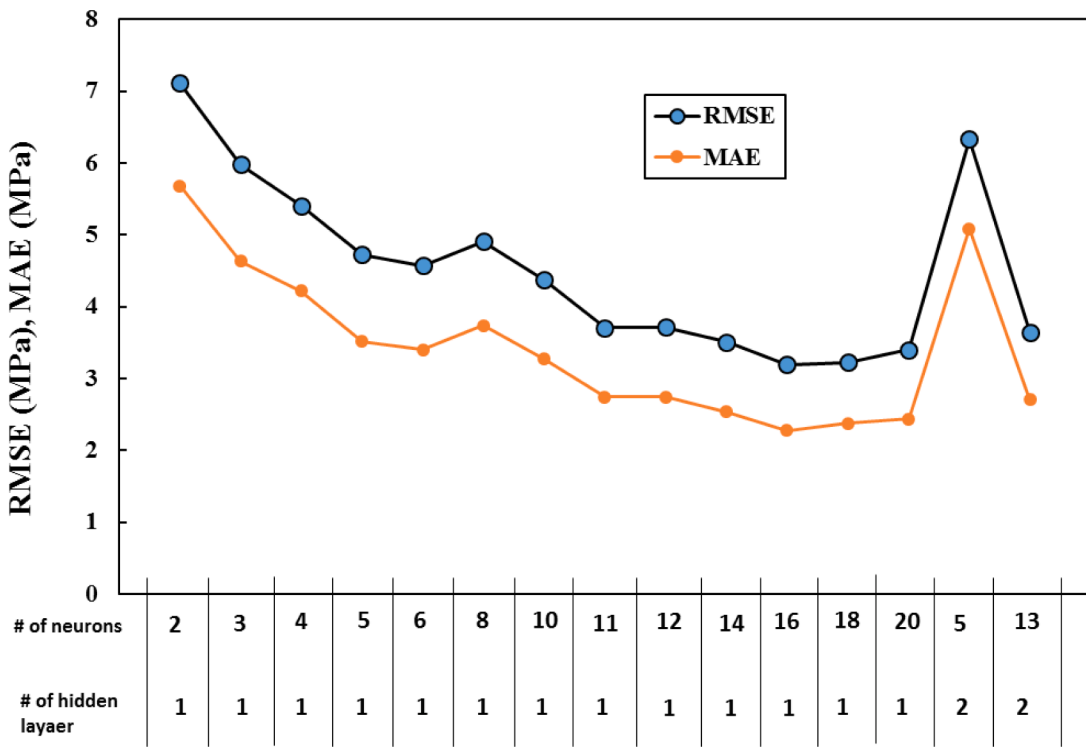


Fig. 8. Choosing best-hidden layer and neurons for Artificial Neural Network Model based on lower RMSE and MAE values.

5.1. Linear relationship model (LR)

This research aimed to develop a model that evaluates the effect of the maximum number of parameters on the f'_c of UHPFRC. Linear regression is a general method for evaluating the compression strength used in this study [40]. But eleven variables were proposed to increase the reliability of the predicted strength value Eq. (1).

$$f'_c = a + b^* \left(\frac{w}{c} \right) + c^*(C) + d^*(W) + e^*(S) + f^*(SP) + g^*(SF) + h^*(t) + \dots \quad (1)$$

Where a to l are model parameters.

5.2. Pure quadratic model

The pure Quadratic technique (model) (Eq. (2)) was used to evaluate the f'_c of UHPFRC as follows:

$$\begin{aligned} f'_c = & \beta_0 + \beta_1^* \left(\frac{w}{c} \right) + \beta_2^*(C) + \beta_3^*(W) + \beta_4^*(S) + \beta_5^*(SP) + \beta_6^*(SF) + \beta_7^*(t) \\ & + \beta_8^*(Fb) + \beta_9^*(AR) + \beta_{10}^*(T) + \beta_{11}^*(FC) + \beta_{12}^* \left(\frac{w^2}{c} \right) + \beta_{13}^*(C^2) \\ & + \beta_{14}^*(W^2) + \beta_{15}^*(S^2) + \beta_{16}^*(SP^2) + \beta_{17}^*(SF^2) + \beta_{18}^*(t^2) + \beta_{19}^*(Fb^2) \\ & + \beta_{20}^*(AR^2) + \beta_{21}^*(T^2) + \beta_{22}^*(FC^2) \end{aligned} \quad (2)$$

Where β_0 to β_{22} are the model constants.

5.3. M5P tree model

The M5P-tree modifies the Quinlan M5 method [41–43]. Tree modeling can manage large amounts of data with multiple dimensions. Node-level error estimates are used to produce M5P-tree division criteria. M5P-tree error is the class's standard deviation. Nodes are separated by the feature that minimizes predicted error reduction after analyzing each attribute. Because of branching, offspring nodes (sub-trees or smaller nodes) have lower SD. Parents (larger nodes) chose the structure that reduces errors the most after evaluating all topologies.

This division's tree-like topology favors overfitting.

5.4. Artificial intelligence (ANN)

Reverse neural networks are ANNs. It has three layers: input, output, and hidden [41,43,44]. The input layer receives the signal. The output layer does prediction and categorization. True ANN engines have hidden layers between input and output. Similar to ANN's feed-forward network, source data goes to the target layer. Multi-hidden layer results improved during trial cycles to find the ideal number for error reduction and R^2 . Due to the complexity of numerous hidden layers, a single hidden layer of 16 neural networks was chosen for this study by trial and error to gain higher performance utilizing statistical measures such as RMSE, MAE, and R^2 . Lower RMSE, MAE, and R^2 indicate that the model performance is well (Fig. 8).

6. Assessment criteria for the developed models

The coefficient of determination (R^2), Root Mean Squared Error (RMSE), Mean Absolute Error (MAE), Scatter Index (SI), and OBJ were used to evaluate the precision and efficiency of the model predictions. Four other models were predicted. All models were assessed using several standard evaluation criteria to compare all models and select the most accurate one, such as: Model validation, lowest residual error, highest R^2 , lower MAE, OBJ, RMSI, and SI values.

Their equations are:

$$R^2 = \left[\frac{\sum_{p=1}^n (y_i - \bar{y})(x_i - \bar{x})}{\sqrt{\left[\sum_{n=1}^n (y_i - \bar{y})^2 \right] \left[\sum_{p=1}^n (x_i - \bar{x})^2 \right]}} \right]^2 \quad (3)$$

$$\text{RMSE} = \sqrt{\frac{\sum_{n=1}^n (y_i - \bar{x}_i)^2}{n}} \quad (4)$$

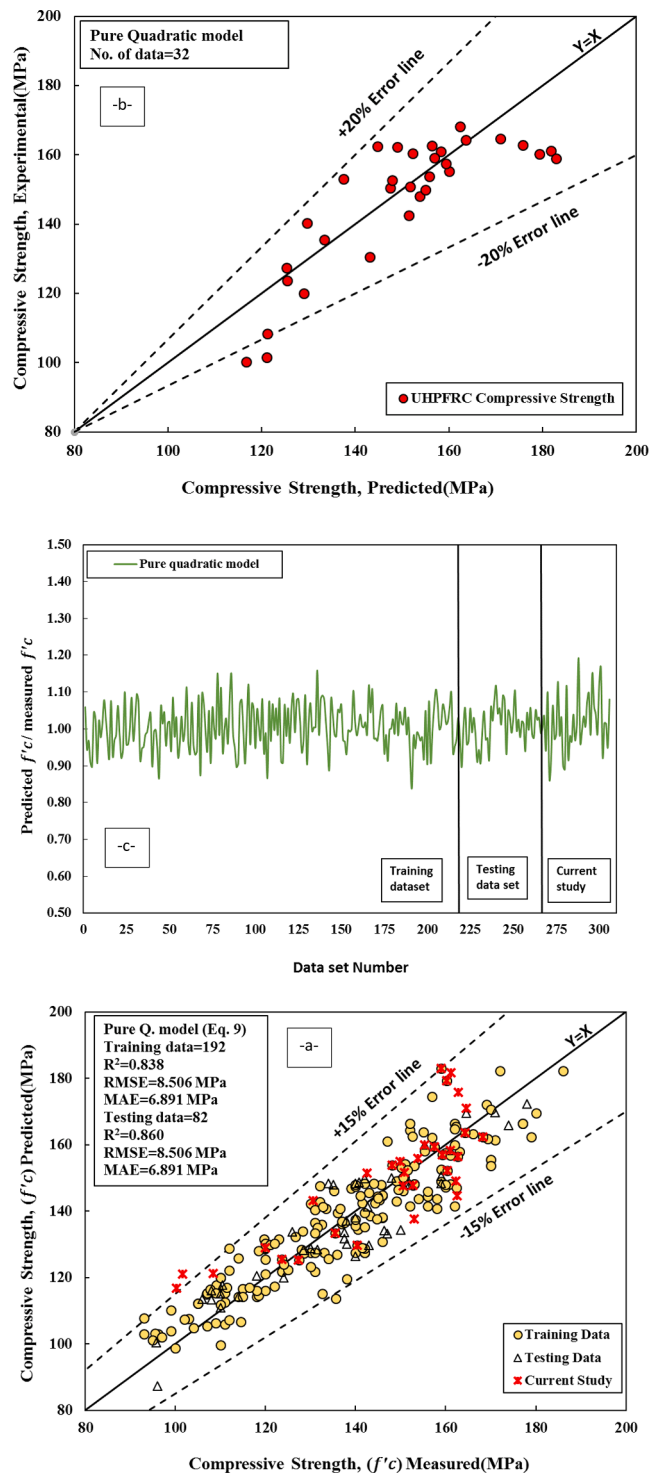
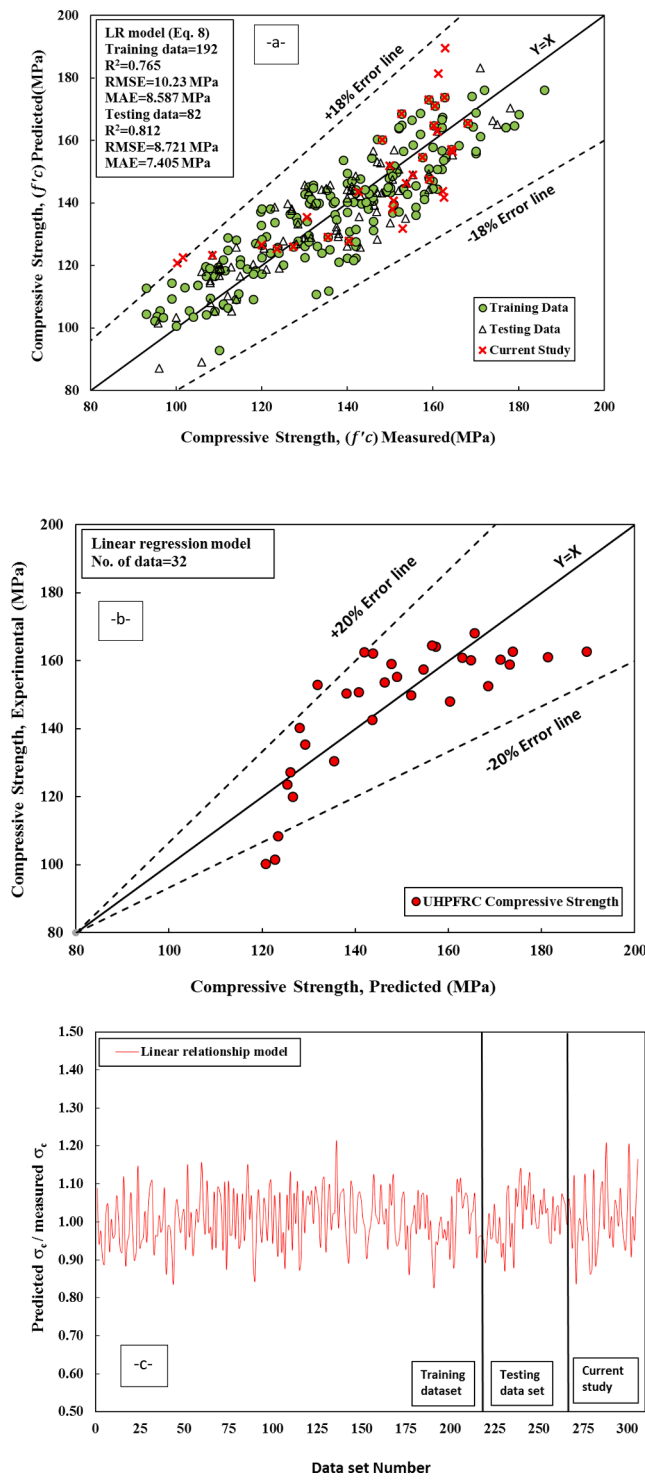


Fig. 9. Comparison between measured and predicted the f'_c of UHPFRC using linear Regression Model (a) model performance, (b) Experimental and Model comparison, and (c) residual error.

Fig. 10. Comparison between measured and predicted the f'_c of UHPFRC using Pure Quadratic Model (a) model performance, (b) Experimental and Model comparison, and (c) residual error.

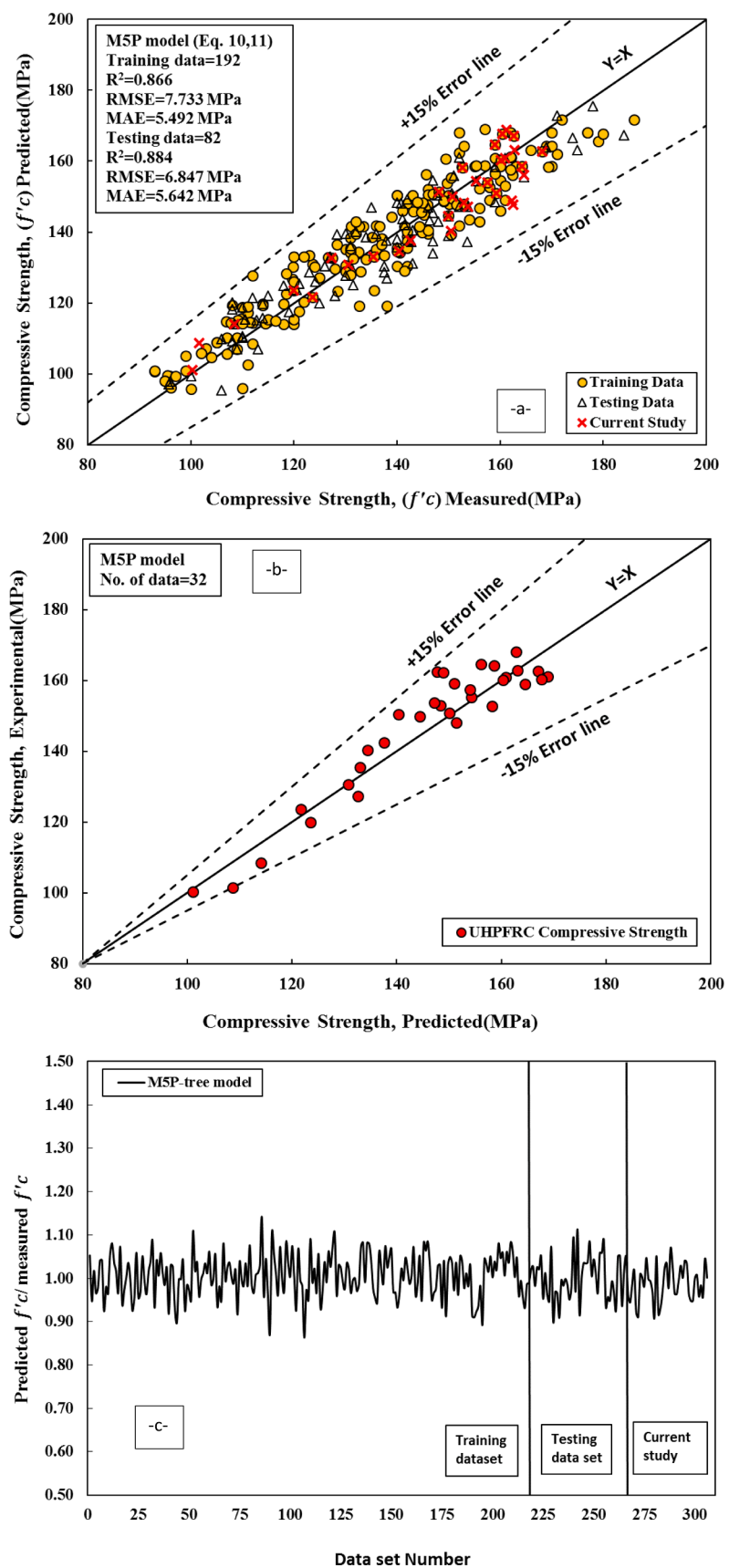


Fig. 11. Comparison between measured and predicted the f'_c of UHPFRC using the M5P-tree Model (a) model performance, (b) Experimental and Model comparison, and (c) residual error.

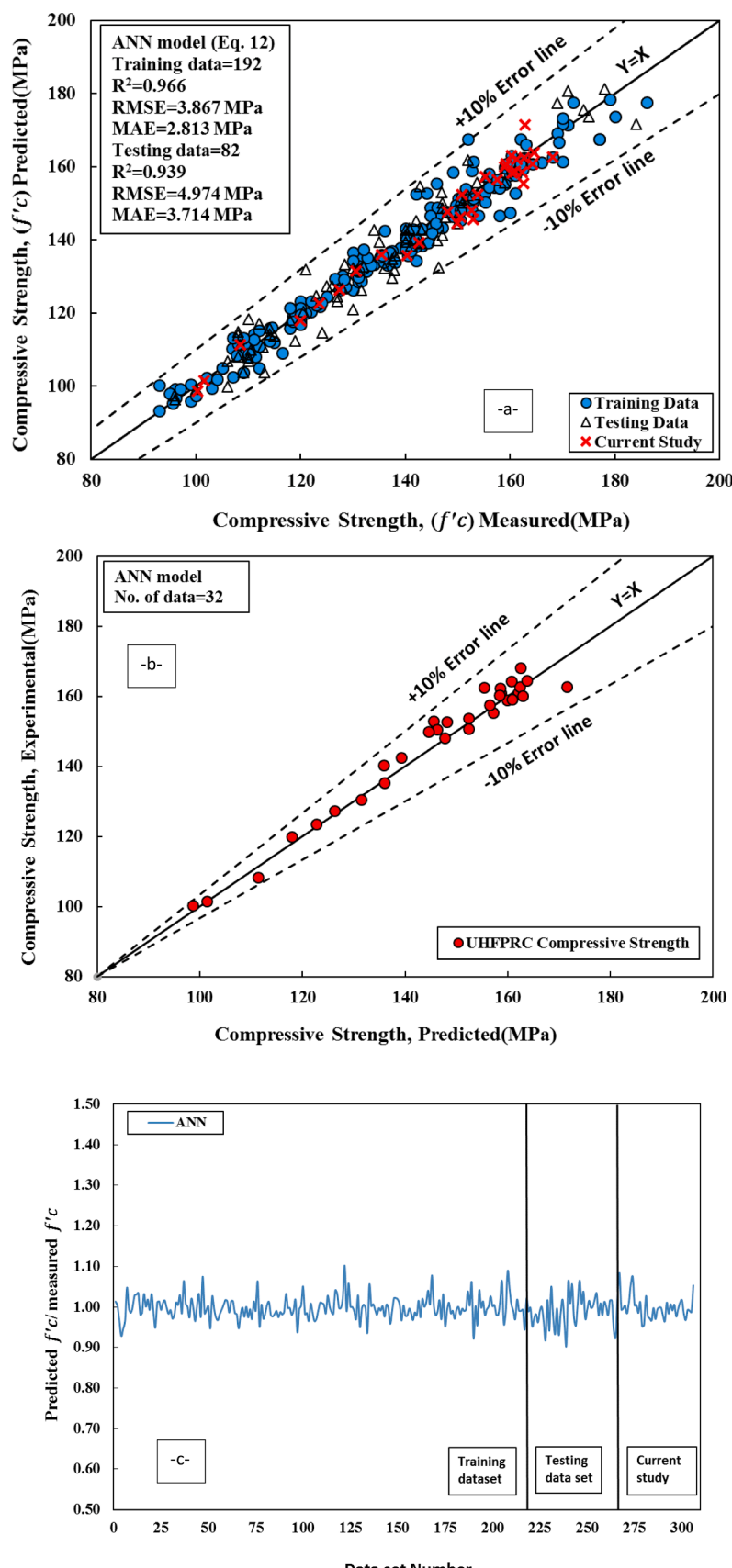


Fig. 12. Comparison between measured and predicted the f'_c of UHPFRC using (a) model performance, (b) Experimental and Model comparison, and (c) residual error.

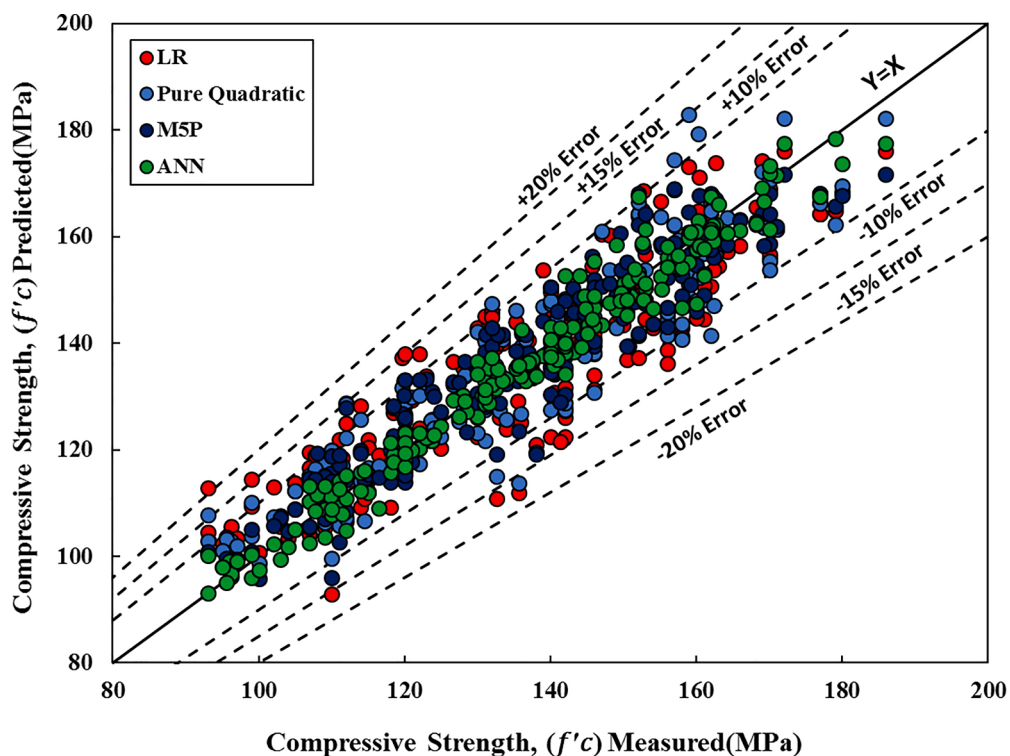


Fig. 13. Comparison between developed models based on variation in predicted compressive with measured compressive strength using the training dataset.

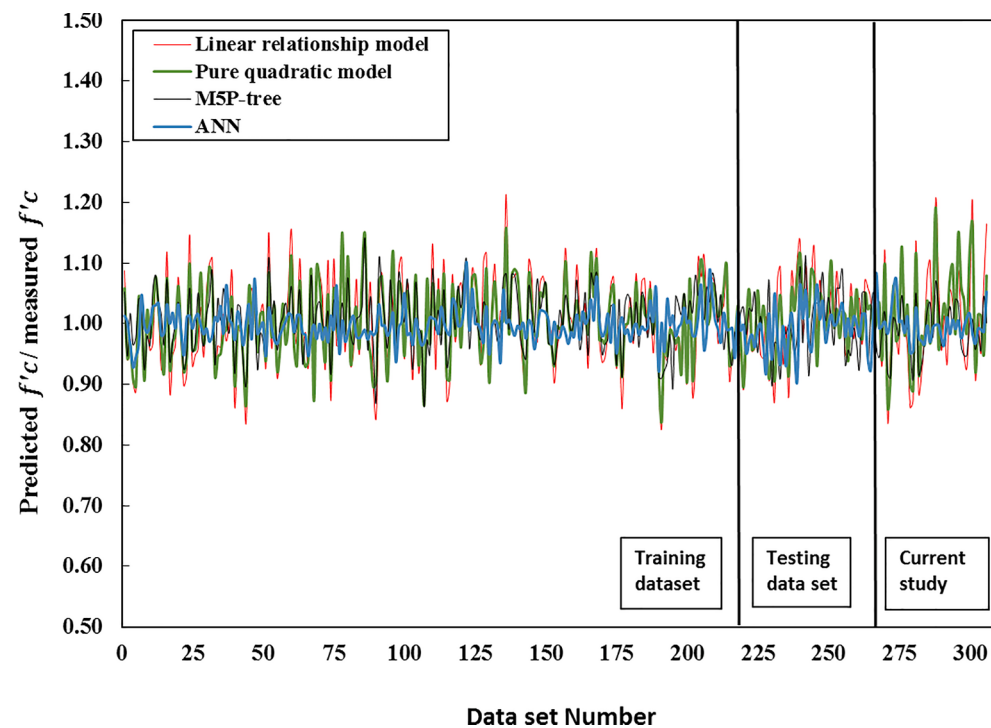


Fig. 14. Residual error of the compressive strength of UHPFRC using training, testing, and experimental dataset.

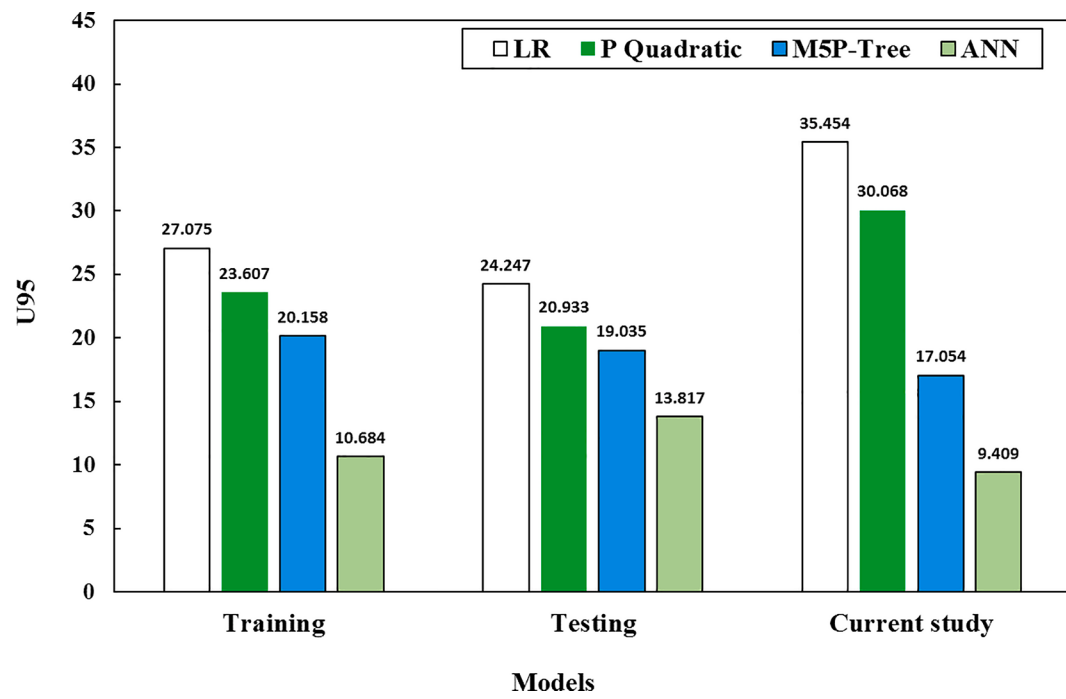


Fig. 15. The U_{95} values for all developed models.

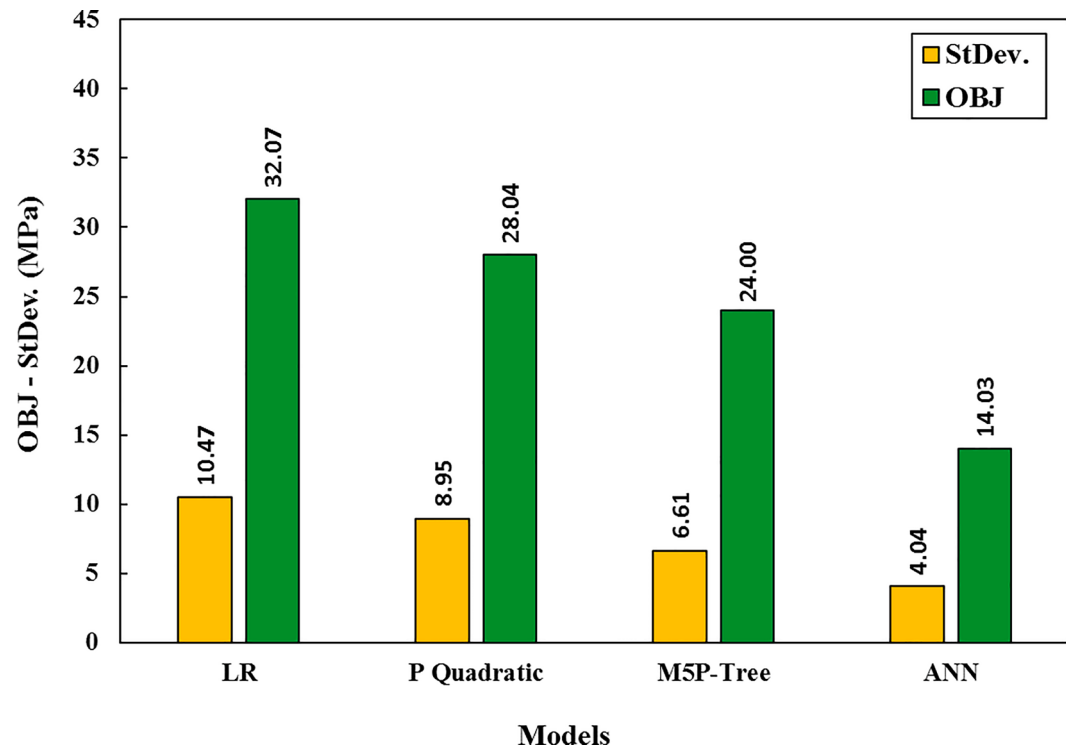


Fig. 16. The OBJ and StDev. values for all developed models.

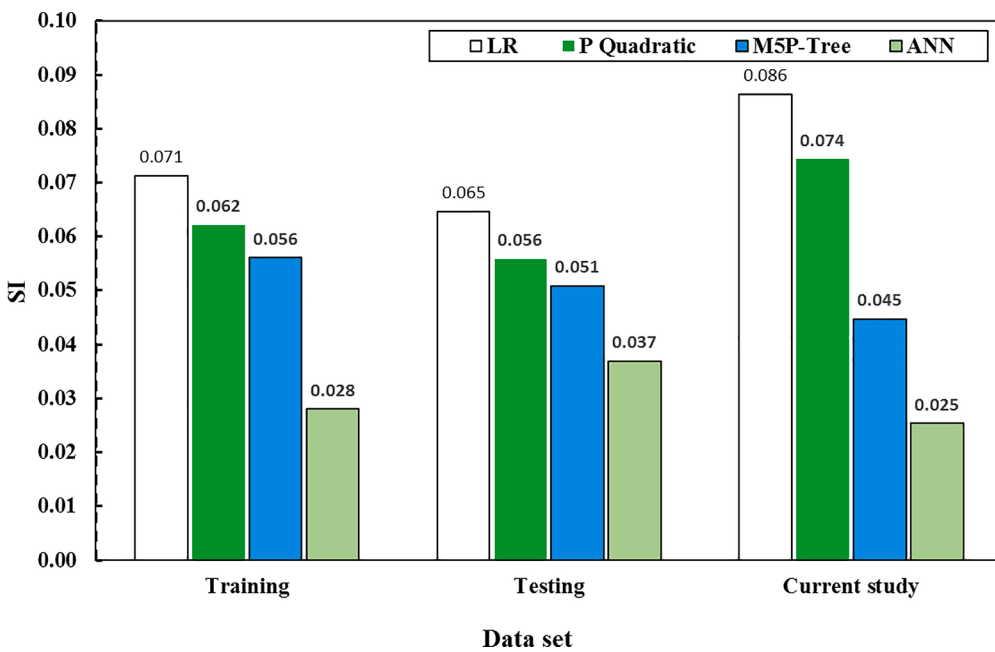


Fig. 17. Comparison of the SI performance parameter of different developed models for the training dataset and testing dataset.

$$\text{MAE} = \frac{\sum_{p=1}^n |(y_i - x_i)|}{n} \quad (5)$$

$$\text{SI} = \frac{RMSE}{yi} \quad (6)$$

$$\text{OBJ} = \left(\frac{n_{tr}}{n_{all}} * \frac{RMSE_{tr} + MAE_{tr}}{R_{tr}^2 + 1} \right) + \left(\frac{n_{tst}}{n_{all}} * \frac{RMSE_{tst} + MAE_{tst}}{R_{tst}^2 + 1} \right) + \left(\frac{n_{val}}{n_{all}} * \frac{RMSE_{val} + MAE_{val}}{R_{val}^2 + 1} \right) \quad (7)$$

y_i = Labrotary tested values; x_i = estimated value; \bar{y} = average of y_i ; \bar{x} = average of x_i , and n is the number of datasets.

7. Analysis and discussion

The growth of compression strength increased rapidly from 7 days to 90 days at all curing temperatures, notably in the 30 and 90 °C curing regimes. During the first week after casting, the compressive strength of the 20, 30, and 90 °C thermally cured specimens increased significantly. It shows that cast-in-situ UHPFRC members can achieve adequate compression strength in a reasonable amount of time. The compression strength gain was approximately 48, 67, and 78 percent for the 10, 20, and 30 °C cured specimens compared to the 90 °C specimens after seven days. Strength gain was reported to be 75, 85, and 96 percent at 28 days and 89, 96, and 97 percent at 90 days for the same concrete mixtures. The results of this study on the development of UHPFRC compressive strength can significantly lower the high initial cost and energy required in precast concrete production.

An application of Dynamic Data Driven Optimization Methodology (DDDOM), which employs concurrent use of simulation and experiment, is presented for the design of the vortex promoter to maximize the heat removal rate from multiple protruding heat sources located in a channel, while keeping the pressure drop within reasonable limits. Concurrent use of computer simulation and experiment in real time is shown to be an effective tool for efficient engineering design and optimization. Numerical simulation can effectively be used for low flow rates and low

heat inputs. However, with transition to oscillatory and turbulent flow at large values of these quantities, the problem becomes more involved and computational cost increases dramatically. Under these circumstances, experimental systems are used to determine the component temperatures for varying heat input and flow conditions. The design variables

are taken as the Reynolds number and the shape and size of the vortex promoter. The problem is a multi-objective design optimization problem, where the objectives are maximizing the total heat transfer rate, as given by the Nusselt number, Nu, and minimizing the pressure drop, ΔP. This multi-objective problem is converted to a single-objective problem by combining the two objective functions of the form Nutota/ΔPb, where a and b are constants [46]. Three one-third scale reinforced concrete (RC) beam-column-slab structure specimen tests were conducted to investigate the collapse mechanisms under a loss of the corner column, including a frame with slab (S-COR), a frame with slab and secondary beams (SS-COR), and a frame without slab (NS-COR). The slab and secondary beam's contributions were investigated by comparing the SS-COR and NS-COR, SS-COR, and S-COR specimens. The results show that the RC slab significantly enhanced the load resistance. Only a slight increase in the peak resistance capacity of the SS-COR specimen was observed, while the ductility improved obviously due to the existence of secondary beams. The failure mode of the SS-COR frame is different from that of the S-COR frame: No concrete failure line occurs on the slab bottom, and the cracks develop entirely on the slab top. Moreover, based on the test results, finite element models (FE) were updated by adapting the OpenSeespy, which shows a good fit between the test curves and simulation results. A 1,000 samples considering the uncertainty parameters were generated using Monte Carlo sampling to better understand the effect of uncertainty on the structure response. Data-driven models based on machine learning were used to predict the peak resistance capacity of the RC structures with slab and secondary beams [47].

Table 3

Transfer functions used in the optimum ANN model.

Nr.	Transfer Function, Equation, and Matlab function	Graph
1	Hyperbolic tangent sigmoid transfer function $a = f(n) = \frac{2}{1 + \exp(-2^n)} - 1$ $a = f(n) = \text{tansig}(n)$	
2	Linear transfer function $a = f(n) = n$ $a = f(n) = \text{purelin}(n)$	

7.1. Linear relationship model (LR)

The connection between measured and predicted f'_c of UHPFRC is shown in Fig. 9(a). The value of each parameter in the existing model was calculated by optimizing the sum of error squares. Eq. (8) represents the final result of all trials.

$$f'_c = 113.65 + 33.4*(w/c) + 0.04*(C) - 0.31*(W) - 0.001*(S) + 0.22*(SP) + 0.01*(SF) + 0.27*(t) + 0.11*(Fb) - 0.004*(AR) + 0.26*(T) - 1.25*(FC) \quad (8)$$

The estimated measured compression strength ratio ranged from 0.82 to 1.21 (Fig. 9b). The w/c has the highest effect on the f'_c of UHPFRC, whereas the sand content has the lowest (Eq. 8). The value for

assessment parameters such as R^2 , RMSE, and MAE is 0.765, 10.23 MPa, and 8.587 MPa. Meanwhile, the values of U_{95} were 27.07, 24.247, and 35.45 for the training, testing, and validated datasets, respectively, as shown in Fig. 15.

7.2. Pure quadratic model (Eq. (9))

In Fig. 10a, the projected f'_c is compared to the measured f'_c produced from UHPFRC training, testing, and validation datasets. As shown in Fig. 10b, the residual error ranged from 0.83 to 1.19. According to this model, the w/c ratio and Fiber content concentration are the most important factors impacting the compression strength of UHPFRC.

$$f'_c = 35 + 141.4*\left(\frac{w}{c}\right) + 0.07*(C) - 0.27*(W) + 0.01*(S) + 0.42*(SP) + 0.14*(SF) + 0.67*(t) + 0.12*(Fb) - 0.02*(AR) + 0.48*(T) - 1.87*(FC) + 0.014*\left(\frac{w^2}{c}\right) - 1.5 \times 10^{-5}*(C^2) - 0.0002*(W^2) - 4.85 \times 10^6*(S^2) - 0.002*(SP^2) - 0.003*(SF^2) - 0.0026*(t^2) - 0.0014*(Fb^2) - 1.8 \times 10^{-5}*(AR^2) - 0.001*(T^2) + 0.52*(FC^2) \quad (9)$$

Table 4
Final values of weights and bias of the optimum ANN-11–16-1 model.

IW{1,1} (16 × 11)	[LW{1,1}] (16 × 1)	[B{1,1}] (1 × 1)	[LW{2,1}] (16 × 1)	[B{2,1}] (1 × 1)
-0.2862	-1.6789	-0.3596	2.9179	2.1581
3.9992	1.1557	3.6863	1.5354	2.2000
3.1683	-0.3070	2.6527	-0.3315	-3.3188
0.9745	0.2306	0.4956	2.1994	8.0805
2.2506	-1.9259	-1.8006	4.7812	-0.8741
0.1024	0.6492	0.3850	0.9670	0.5453
1.9989	1.7765	4.5942	6.7628	3.5483
1.6121	0.1789	1.1012	2.2414	0.8919
-0.6286	3.9439	-0.3961	0.9568	0.0452
0.2947	3.1674	1.7351	-0.1260	-0.0676
-1.4138	1.4470	1.3404	3.3242	1.7471
-0.7101	1.4370	-2.2418	3.6448	6.8012
2.5067	0.5016	3.8179	-0.3755	-2.2254
2.1007	-2.0123	-2.2972	-4.8754	-2.5505
1.5546	-2.2717	-2.6654	-7.6332	2.3979
-0.0203	-0.0083	-0.0420	-2.2818	-0.5836
			2.3873	1.9226
				0.6364
			0.2848	-2.4301
				2.6698
				-3.6767
				-2.1200
				0.3428

[IW{1,1}] is the matrix of weight values between the input layer and the first hidden layer,
 [LW{1,1}] is the matrix of weight values between the 1st hidden Layer and the Output Layer.
 [B{1,1}] is the matrix of bias values for the hidden layer,
 [B{2,1}] is the matrix of bias values for the output layer.

The R^2 and RMSE for the Eq. (9) are 0.838 and 8.506 MPa. The OBJ and scatter index for the proposed model are 28.04 MPa and 0.062, respectively, for training datasets.

7.3. M5P tree model

The M5P tree model was developed by [46]. The M5P-tree model is utilized to forecast the UHPFRC compressive strength by using 274 data collected from previous studies for training and testing and 32 experimental laboratory data for validation prediction [42–45]. The training, testing, and validation (experimental data) sets were assessed using various prediction accuracy indexes (R^2 , MAE, RMSE, SI). Fig. 11 shows the expected vs measured compressive strength. The developed model has a 15 % error line, meaning all measured compressive strength falls within that range. This model's R^2 is 0.866, better than the LR and pure quadratic models. The M5P model RMSE, MAE, SI, and OBJ function indexes registered the following values, respectively 7.733 MPa, 5.492 MPa, 0.056, and 24 MPa (Figs. 16 and 17).

Age (days) $<= 14$ use LM1.

Age (days) greater than 14 use LM2.

LM num: 1.

$$f_c' = 65.175 * w/c + 0.0063 * C - 0.1756 * W + 0.2007 * SP + 1.4205 * t + 0.1261 * F + 0.3807 * T + 118.8463 (10).$$

LM num: 2.

$$f_c' = 0.0219 * C - 0.2277 * W + 0.274 * SP + 0.0161 * SF + 0.2 * t + 0.0913 * F + 0.2342 * T + 124.1994 (11).$$

7.4. Artificial neural networks (ANN)

Input parameters were supplied to the network for training, testing, and validation. Creating an ANN model is an iterative process (Fig. 11). It is crucial to choose appropriate input variables [46–51]. They should contain all necessary information regarding the goal values. This study used 11 different characteristics to estimate UHPFRC's compressive strength. This study used 19 neural networks to represent hidden layers. The training duration is 50,000, and the learning rate is 0.1. The number of epochs influences how often the learning algorithm processes the training dataset. The more epochs, the higher the R^2 , the lower the RMSE, and the lower the MAE. The projected vs actual value of f_c' is shown in Fig. 12. The number of epochs also indicates how many times the learning algorithm can process the training dataset. The more epochs, the greater the R^2 , and the lower the RMSE and the MAE. The ANN model predicts UHPFRC compressive strength better than the (LR, M5P-tree, and pure quadratic) models. The model's R^2 , RMSE, and MAE are 0.966, 3.867, and 2.813 MPa. The current model's SI value for the training dataset is 0.025. (Fig. 17).

7.5. A closed-form equation for the estimation of concrete compressive strength based on the optimum ANN model

It is common for most published studies about the studied problem to present the architecture of the resulting optimal artificial neural network model primarily, together with the values of the statistical indicators based on which the model performance was evaluated. Yet, this information alone makes it impossible to assess the proposed mathematical model reliability and, more importantly, prohibits any substantial comparison with other models available in the literature. To assess the reliability of the proposed computational model, the researchers must provide all the pertinent data that clearly describe the model so that it can be reproduced and checked by other researchers. Especially in the case of artificial neural networks, apart from the architecture. The transfer functions corresponding to the suggested ANN model and the final values of weights and biases of their generated and proposed models are thought necessary. This study presents the explicit mathematical equation for the optimum developed ANN model and weights and biases values to overcome this deficiency. Therefore, it can

Table 5

Typical percentage of error of the proposed models based on the experimental laboratory data.

Sample no.	LR model			Pure Quadtratic model			M5P tree model			ANN model		
	Experimental f'_c , (MPa)	Predicted f'_c , (MPa)	% of error	Experimental f'_c , (MPa)	Predicted f'_c , (MPa)	% of error	Experimental f'_c , (MPa)	Predicted f'_c , (MPa)	% of error	Experimental f'_c , (MPa)	Predicted f'_c , (MPa)	% of error
1	135.45	129.17	4.86	135.45	133.37	1.56	135.45	133.006	1.84	135.45	135.93	0.35
2	161.20	181.37	11.12	161.20	181.73	11.30	161.2	168.813	4.51	161.2	162.03	0.51
3	161.00	162.89	1.16	161.00	158.21	1.77	161	160.833	0.10	161	158.6	1.51
4	155.30	148.94	4.27	155.30	159.99	2.93	155.3	154.278	0.66	155.3	157.2	1.21
5	152.95	131.81	16.04	152.95	137.52	11.22	152.95	148.292	3.14	152.95	145.57	5.07
6	162.53	141.84	14.59	162.53	144.67	12.35	162.53	147.725	10.02	162.53	155.34	4.63
7	108.45	123.36	12.09	108.45	121.14	10.48	108.45	114.004	4.87	108.45	111.38	2.63
8	162.28	143.77	12.87	162.28	149.00	8.91	162.28	148.806	9.05	162.28	158.48	2.40
9	150.50	138.01	9.05	150.50	147.51	2.03	150.5	140.305	7.27	150.5	146.21	2.93
10	168.20	165.53	1.61	168.20	162.36	3.60	168.2	162.795	3.32	168.2	162.51	3.49
11	148.10	160.25	7.58	148.10	153.79	3.70	148.1	151.305	2.12	148.1	147.68	0.28
12	152.70	168.54	9.40	152.70	147.82	3.30	152.7	158.147	3.44	152.7	148.07	3.12
13	157.50	154.60	1.88	157.50	159.41	1.20	157.5	153.99	2.28	157.5	156.5	0.64
14	101.60	122.66	17.17	101.60	121.06	16.08	101.6	108.733	6.56	101.6	101.42	0.17
15	162.70	173.82	6.40	162.70	156.39	4.03	162.7	167.054	2.61	162.7	162.33	0.22
16	164.30	157.24	4.49	164.30	163.56	0.45	164.3	158.537	3.64	164.3	160.71	2.23
17	149.90	151.96	1.35	149.90	154.99	3.28	149.9	144.462	3.76	149.9	144.625	3.65
18	150.80	140.65	7.22	150.80	151.66	0.57	150.8	150.02	0.52	150.8	152.41	1.06
19	119.95	126.53	5.20	119.95	128.95	6.98	119.95	123.478	2.86	119.95	117.936	1.71
20	130.60	135.37	3.53	130.60	143.09	8.73	130.6	130.777	0.14	130.6	131.466	0.66
21	127.35	126.00	1.07	127.35	125.30	1.64	127.35	132.585	3.95	127.35	126.248	0.87
22	159.00	173.07	8.13	159.00	182.93	13.08	159	164.555	3.38	159	159.879	0.55
23	142.60	143.66	0.74	142.60	151.42	5.83	142.6	137.619	3.62	142.6	139.197	2.44
24	164.60	156.49	5.18	164.60	171.03	3.76	164.6	156.038	5.49	164.6	163.744	0.52
25	159.20	147.64	7.83	159.20	156.89	1.47	159.2	150.97	5.45	159.2	160.84	1.02
26	160.23	164.78	2.76	160.23	179.36	10.67	160.23	160.296	0.04	160.23	162.944	1.67
27	100.30	120.72	16.92	100.30	116.73	14.07	100.3	101.091	0.78	100.3	98.655	1.67
28	140.35	127.94	9.70	140.35	129.63	8.27	140.35	134.487	4.36	140.35	135.757	3.38
29	123.60	125.30	1.35	123.60	125.48	1.50	123.6	121.646	1.61	123.6	122.659	0.77
30	153.75	146.30	5.09	153.75	155.84	1.34	153.75	147.148	4.49	153.75	152.315	0.94
31	160.40	171.18	6.30	160.40	152.24	5.36	160.4	167.676	4.34	160.4	158.353	1.29
32	162.80	189.66	14.16	162.80	175.76	7.38	162.8	163.072	0.17	162.8	171.438	5.04

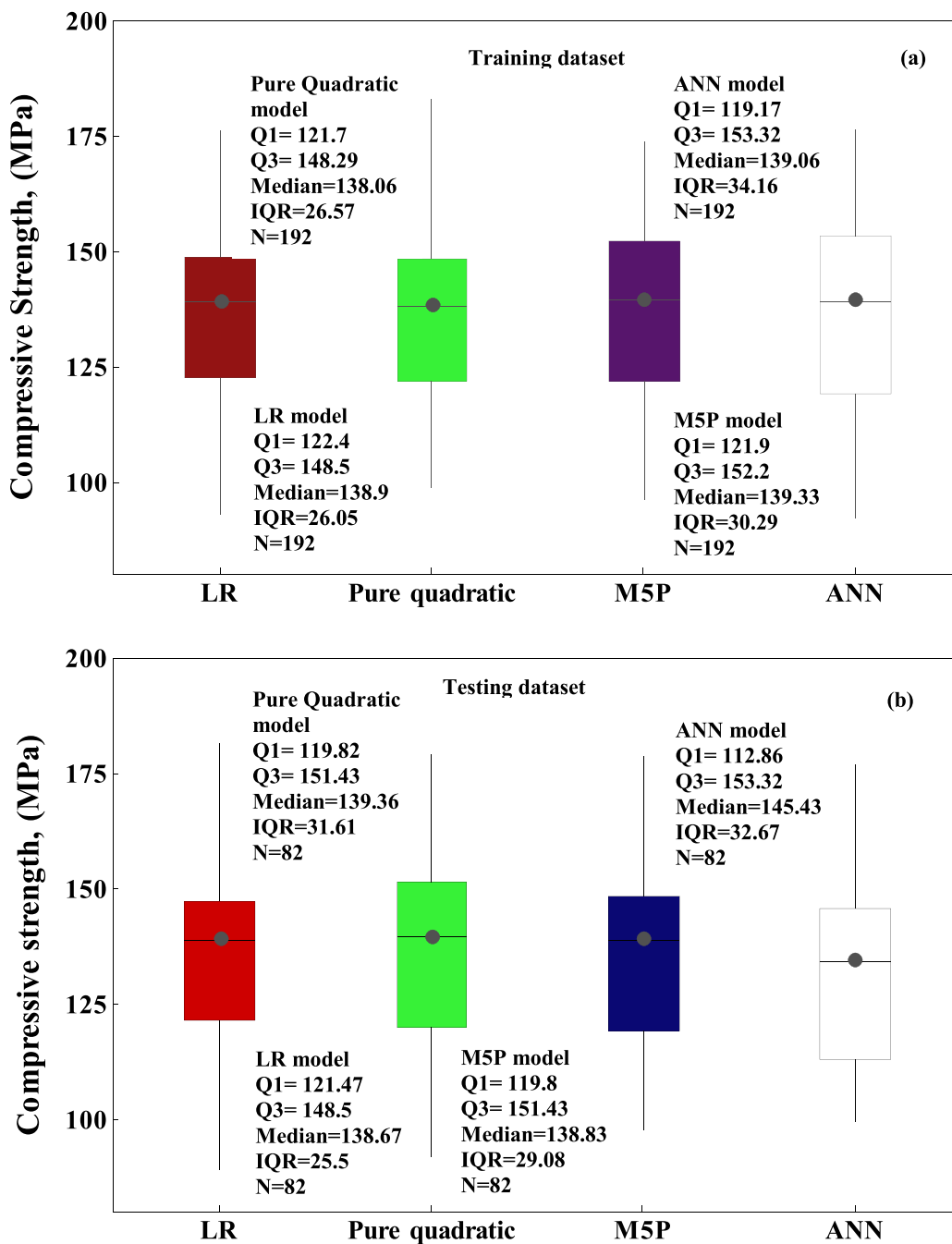


Fig. 18. Box Plot of predicted compressive strength of UHPFRC using different models (a) training dataset, and (b) testing dataset.

be readily implemented in a spreadsheet environment, by the interested reader, even without prior expertise in Artificial Neural Networks.

In light of the above, the derived equation for the prediction of the UHPFRC compressive strength (f'_c), using the eleven input parameters (w/c, c, w, S, SP, SF, t, F, AT, T, and FC), is expressed by the following equation:

$$f'_c = \text{purelin}([\text{LW}\{2,1\}] \times [\text{tansig}([\text{IW}\{1,1\}] \times [\text{IP.}] + [\text{B}\{1,1\}]) + [\text{B}\{2,1\}]) \quad (12)$$

where the linear and hyperbolic tangent sigmoid transfer functions are purelin and tansig. Table 3 shows both their equations and graphs in

detail. $[\text{IW}\{1,1\}]$ is a 16×11 matrix containing the hidden layer weights; $[\text{LW}\{2,1\}]$ is a 1×16 vector containing the output layer weights; $[\text{IP.}]$ is an 11×1 vector containing the eleven input variables; $[\text{B}\{1,1\}]$ is a 16×1 vector representing the hidden layer bias; and $[\text{B}\{2,1\}]$ is a 1×1 vector containing the output layer bias. Equation (12) is a completely mathematical representation of the established ANN model, making it more practical for engineers and researchers to employ.

The $[\text{IP.}]$ the vector that contains the 11 input parameters is expressed as:

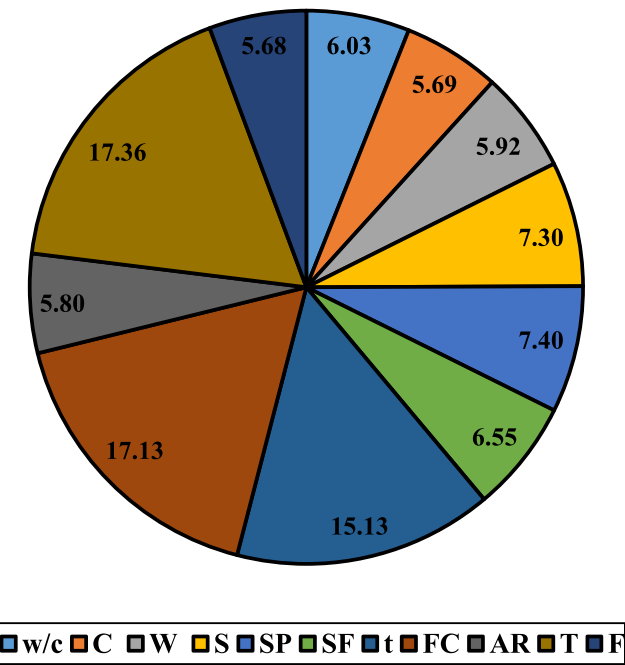


Fig. 19. Sensitivity analysis to investigate the effect of input variables on the f'_c based on RMSE by using the ANN model.

$$[IP.] = \begin{bmatrix} w/c \\ c \\ w \\ S \\ SP \\ SF \\ t \\ F \\ AT \\ T \\ FC \end{bmatrix} \quad (13)$$

The values of the bias and final weights that determine the matrices $[IW\{1, 1\}]$, $[LW\{2, 1\}]$, $[B\{1, 1\}]$ and $[B\{2, 1\}]$ are presented in Table 4.

7.6. Comparison between developed models

The efficiency of the proposed innovative models was assessed using five statistical metrics (R^2 , MAE, RMSE, U_{95} , OBJ, and SI). In comparison to the LR, Pure Quadratic, and M5P-tree models, the ANN model had the lowest RMSE and MAE as well as the highest R^2 values. The maximum error percentage of the ANN model was 5.07 % less than LR, pure quadratic, and M5P models, respectively, as summarized in Table 5. Fig. 13 shows the predicted f'_c vs actual value of all the developed model. The residual error for all models employing training, testing, and validating data sets is shown in Fig. 14, suggesting that the ANN model outperforms other models. As demonstrated in Fig. 15, the ANN model has the lowest U_{95} values compared to other training, testing, and validation datasets.

The OBJ values for all developed models are shown in Fig. 16. The model performs remarkably well at predicting the f'_c of UHPFRC, as evidenced by the lower OBJ values 32.07, 28.04, 24, and 14.03, are the values of OBJ for the LR, Pure Quadratic, M5P, and ANN, respectively. The ANN model has a 56 % lower OBJ value than the LR model, a 50 percent lower value than the Pure Quadratic model, and a 41.6 percent

lower value than the M5P model. This also demonstrates that the ANN model is more efficient and reliable when estimating the compressive strength of UHPFRC mixes.

Fig. 17 depicts the SI assessment parameter values for the proposed models during the training, validating, and testing phases. As shown in Fig. 17, the SI values for all models and stages (training, testing, and validating) were less than 0.1, indicating that all models performed well. Furthermore, the ANN model has lower SI values than other models, just like the other performance variables. The ANN model had lower SI value values in all phases than the LR model, including a reduction of 60 percent in training, reduction of 43 percent in testing, and 71 percent in the validation data set.

Finally, the M5P-tree model has a 9.6 percent lower SI value in the training phase, an 8.9 percent lower SI value in the testing phase, and a 64 percent lower SI value in the validating dataset than the pure quadratic model. This also demonstrated that the tree model is more efficient and performs better when predicting the compressive strength of UHPFRC mixtures than the LR and Pure quadratic model M.

The box plot in Fig. 18 was also utilized to validate the model's performance for conventional concrete's measured and projected compressive strength. A box plot is built between the first and third quartiles. The whiskers reach both the box minimum and maximum values. It displays how data are skewed or symmetrical around the median. The ANN model outperformed the others.

The ANN model had the highest prediction accuracy of the UHPFRC, as shown in Fig. 15. Table 5 presents experimental and predicted values by the optimum ANN model, allowing independent researchers to verify the stated results.

7.7. Sensitivity investigation

A sensitivity test was performed on the models to determine and assess the most influencing variable that affects the f'_c of UHPFRC combinations [41]. The ANN model was used to analyze sensitivity, an efficient method. Sensitivity analysis was carried out using several distinct training data sets, each with a single input variable extracted. The assessment parameters for each training dataset, such as R^2 , RMSE, and MAE, were established individually. The data show that the curing temperature, fiber content, and curing time are the most important variables affecting UHPFRC compressive strength. As a result, increasing the curing time and fiber content enhanced the f'_c significantly. The impact of mix proportions on the f'_c of UHPFRC is shown in Fig. 18. Based on the experimental laboratory data and data collection values, the curing temperature had the highest and smallest effect on the UHPFRC compressive strength (Fig. 19) is in line with the observations reported by [12].

8. Conclusions

To find a reliable model to predict the UHPFRC compressive strength, 306 data samples were collected from previous studies and tested in the laboratory. According to the experimental laboratory work and the collected data, the following can be drawn:

1. Within 7 days and up to 90 days of curing, ultimate strength was achieved at 90 °C curing temperature. For 360 days, the specimens gained strength, matching or even exceeding the strength of the specimens that were cured at 90 °C.
2. The fiber content ranged between 0 and 6 %, the curing time between 3 and 180 days, and the sand content between 292–1923 kg/m³. The average fiber content for the production of UHPFRC was 2 %.
3. At 28 days of curing, the average UHPFRC compressive strength was 140.1 MPa. The compressive strength of UHPFRC increased with increasing curing temperature.

4. The correlation matrix showed that the compressive strength of UHPFRC and the mix proportions are not strongly correlated.
5. The ANN model outperformed the prediction accuracy of all the other soft computing models developed for the predictions of the UHPFRC (LR model, pure quadratic model, M5P-tree).
6. The SI values were less than 0.1 for all the developed models and testing stages, indicating the significant prediction accuracy of all the models developed in this research. The ANN model registered the lowest SI value during all testing phases.
7. The ANN model registered the lowest U_{95} values compared to other training, testing, and validation datasets. The ANN model OBJ value was 56 % lower than that of the LR model, 50 % lower than that of the Pure Quadratic, and 46.1 % lower than that of the M5P-tree models.
8. The experimental results and sensitivity analysis revealed that the curing temperature is the essential input parameter that affects the improvement rate and predicts the compressive strength of UHPFRC.
9. The experimental data were matched with the collected data, and the model performances were in good agreement.

Declaration of Competing Interest

The authors declare that they have no known competing financial interests or personal relationships that could have appeared to influence the work reported in this paper.

References

- [1] Máca P, Sovják R, Konvalinka P. Mix design of UHPFRC and its response to projectile impact. *Int J Impact Eng* 2014;63:158–63. <https://doi.org/10.1016/j.ijimpeng.2013.08.003>.
- [2] Hassan AMT, Mahmud GH, Mohammed AS, Jones SW. The influence of normal curing temperature on the compressive strength development and flexural tensile behaviour of UHPFRC with vipulanandan model quantification. *Structures* 2021;30:949–59.
- [3] Mosaberpanah MA, Eren O. Effect of density on compressive strength of ultra high-performance fiber reinforced concrete (UHPFRC) using design of experiment. In: Solid State Phenomena, Vol. 249. Trans Tech Publications Ltd.; 2016. p. 119–24. <https://doi.org/10.4028/www.scientific.net/SSP.249.119>.
- [4] Alsalmam A, Dang CN, Prinz GS, Hale WM. Evaluation of modulus of elasticity of ultra-high performance concrete. *Constr Build Mater* 2017;153:918–28. <https://doi.org/10.1016/j.conbuildmat.2017.07.158>.
- [5] Yang SL, Millard SG, Soutsos MN, Barnett SJ, Le TT. Influence of aggregate and curing regime on the mechanical properties of ultra-high performance fibre reinforced concrete (UHPFRC). *Constr Build Mater* 2009;23(6):2291–8. <https://doi.org/10.1016/j.conbuildmat.2008.11.012>.
- [6] Yang IH, Joh C, Kim BS. Structural behavior of ultra high performance concrete beams subjected to bending. *Eng Struct* 2010;32(11):3478–87. <https://doi.org/10.1016/j.engstruct.2010.07.017>.
- [7] Nguyen N-H, Vo TP, Lee S, Asteris PG. Heuristic algorithm-based semi-empirical formulas for estimating the compressive strength of the normal and high performance concrete. *Constr Build Mater* 2021;304:124467. <https://doi.org/10.1016/j.conbuildmat.2021.124467>.
- [8] Asteris PG, Kolovos KG, Douvika MG, Roinos K. Prediction of self-compacting concrete strength using artificial neural networks. *Eur J Environ Civ Eng* 2016;20(sup1):s102–22.
- [9] Asteris PG, Kolovos KG. Self-compacting concrete strength prediction using surrogate models. *Neural Comput Appl* 2019;31(1):409–24.
- [10] Asteris PG, Ashrafiyan A, Rezaie-Balf M. Prediction of the compressive strength of self-compacting concrete using surrogate models. *Comput Concr* 2019;24(2):137–50.
- [11] Corinaldesi V, Moriconi G. Mechanical and thermal evaluation of ultra high performance fiber reinforced concretes for engineering applications. *Constr Build Mater* 2012;26(1):289–94. <https://doi.org/10.1016/j.conbuildmat.2011.06.023>.
- [12] Hassan AM. Ultra high performance fibre reinforced concrete for highway bridge applications. University of Liverpool; 2013. Doctoral dissertation.
- [13] Magureanu C, Sosa I, Negruțiu C, Héghes B. Physical and mechanical properties of ultra high strength fiber reinforced cementitious composites. Korea Concrete Institute: Fracture Mechanics of Concrete and Concrete Structures; 2010. p. 1497–11491.
- [14] Karim, F. R., Abu Bakar, B. H., Kok Keong, C., & Aziz, O. Q. Influence of fibre size on the compressive strength of ultra-high performance concrete.
- [15] Kang ST, Lee Y, Park YD, Kim JK. Tensile fracture properties of an Ultra High Performance Fiber Reinforced Concrete (UHPFRC) with steel fiber. *Compos Struct* 2010;92(1):61–71. <https://doi.org/10.1016/j.compstruct.2009.06.012>.
- [16] Kwon S, Nishiwaki T, Kitaka T, Mihashi H. Development of ultra-high-performance hybrid fiber-reinforced cement-based composites. *ACI Mater J* 2014;111(3):309.
- [17] Wu Z, Shi C, He W, Wu L. Effects of steel fiber content and shape on mechanical properties of ultra high performance concrete. *Constr Build Mater* 2016;103:8–14. <https://doi.org/10.1016/j.conbuildmat.2015.11.028>.
- [18] Abbas S, Soliman AM, Nehdi ML. Exploring mechanical and durability properties of ultra-high performance concrete incorporating various steel fiber lengths and dosages. *Constr Build Mater* 2015;75:429–41. <https://doi.org/10.1016/j.conbuildmat.2014.11.017>.
- [19] Nguyen DL, Ryu GS, Koh KT, Kim DJ. Size and geometry dependent tensile behavior of ultra-high-performance fiber-reinforced concrete. *Compos B Eng* 2014;58:279–92. <https://doi.org/10.1016/j.compositesb.2013.10.072>.
- [20] Yoo DY, Kang ST, Yoon YS. Effect of fiber length and placement method on flexural behavior, tension-softening curve, and fiber distribution characteristics of UHPFRC. *Constr Build Mater* 2014;64:67–81. <https://doi.org/10.1016/j.conbuildmat.2014.04.007>.
- [21] Song Q, Yu R, Shui Z, Wang X, Rao S, Lin Z. Optimization of fibre orientation and distribution for a sustainable ultra-high performance fibre reinforced concrete (UHPFRC): experiments and mechanism analysis. *Constr Build Mater* 2018;169:8–19. <https://doi.org/10.1016/j.conbuildmat.2018.02.130>.
- [22] Graybeal, B. A. (2006). Material property characterization of ultra-high performance concrete (No. FHWA-HRT-06-103). United States. Federal Highway Administration, Office of Infrastructure Research and Development.
- [23] Krahl PA, Carrazedo R, El Debs MK. Mechanical damage evolution in UHPFRC: experimental and numerical investigation. *Eng Struct* 2018;170:63–77. <https://doi.org/10.1016/j.engstruct.2018.05.064>.
- [24] Hassan AMT, Jones SW, Mahmud GH. Experimental test methods to determine the uniaxial tensile and compressive behaviour of ultra high performance fibre reinforced concrete (UHPFRC). *Constr Build Mater* 2012;37:874–82. <https://doi.org/10.1016/j.conbuildmat.2012.04.030>.
- [25] Yu R, Spiesz P, Brouwers HJH. Mix design and properties assessment of ultra-high performance fibre reinforced concrete (UHPFRC). *Cem Concr Res* 2014;56:29–39. <https://doi.org/10.1016/j.cemconres.2013.11.002>.
- [26] Ashekezari GD, Fotouhi F, Razmara M. Experimental relationships between steel fiber volume fraction and mechanical properties of ultra-high performance fiber-reinforced concrete. *J Build Eng* 2020;32:101613. <https://doi.org/10.1016/j.jobe.2020.101613>.
- [27] Aghayari, R., & Al-Mwanes, A. O. (2019). An Experimental Investigation of Mechanical Properties of The Ultra-High Performance Fiber Reinforced Concrete (UHPFRC).
- [28] Jin L, Zhang R, Tian Y, Dou G, Du X. Experimental investigation on static and dynamic mechanical properties of steel fiber reinforced ultra-high-strength concretes. *Constr Build Mater* 2018;178:102–11. <https://doi.org/10.1016/j.conbuildmat.2018.05.152>.
- [29] Mohammed BH, Sherwani AFH, Faraj RH, Qadir HH, Younis KH. Mechanical properties and ductility behavior of ultra-high performance fiber reinforced concretes: effect of low water-to-binder ratios and micro glass fibers. *Ain Shams Eng J* 2021;12(2):1557–67.
- [30] Alsalmam A, Dang CN, Martí-Vargas JR, Hale WM. Mixture-proportioning of economical UHPC mixtures. *J Build Eng* 2020;27:100970. <https://doi.org/10.1016/j.jobe.2019.100970>.
- [31] Prem PR, Bharatkarum BH, Iyer NR. Influence of curing regimes on compressive strength of ultra high performance concrete. *Sadhana* 2013;38(6):1421–31.
- [32] Meng W, Khayat KH. Effect of hybrid fibers on fresh properties, mechanical properties, and autogenous shrinkage of cost-effective UHPC. *J Mater Civ Eng* 2018;30(4):04018030. [https://doi.org/10.1061/\(ASCE\)MT.1943-5533.0002212](https://doi.org/10.1061/(ASCE)MT.1943-5533.0002212).
- [33] Prem PR, Bharatkarum BH, Iyer NR. Mechanical properties of ultra high performance concrete. *World Acad Sci Eng Technol* 2012;68:1969–78.
- [34] Ahmad S, Hakeem I, Azad AK. Effect of curing, fibre content and exposures on compressive strength and elasticity of UHPC. *Adv Cem Res* 2015;27(4):233–9. <https://doi.org/10.1680/adcr.13.00090>.
- [35] Sovják R, Máca P, Imlauf T. Effect of fibre aspect ratio and fibre volume fraction on the effective fracture energy of ultra-high-performance fibre-reinforced concrete. *Acta Polytech* 2016;56(4):319–27. <https://doi.org/10.14311/AP.2016.56.0319>.
- [36] Yousef AM, Tahwia AM, Marami NA. Minimum shear reinforcement for ultra-high performance fiber reinforced concrete deep beams. *Constr Build Mater* 2018;184:177–85. <https://doi.org/10.1016/j.conbuildmat.2018.06.022>.
- [37] Ahmad S, Hakeem I, Masleehuddin M. Development of UHPC mixtures utilizing natural and industrial waste materials as partial replacements of silica fume and sand. *Sci World J* 2014;2014:1–8.
- [38] Bahmani H, Mostofinejad D, Dadvar SA. Effects of synthetic fibers and different levels of partial cement replacement on mechanical properties of UHPFRC. *J Mater Civ Eng* 2020;32(12):04020361. [https://doi.org/10.1061/\(ASCE\)MT.1943-5533.0003462](https://doi.org/10.1061/(ASCE)MT.1943-5533.0003462).
- [39] Al-Mwanes AO, Agayari R. Studying the effect of hybrid fibers and silica fumes on mechanical properties of ultra-high-performance concrete. *IOP Conf Ser: Mater Sci Eng* 2021;1076(1):012128.
- [40] Zain MFM, Abd SM. Multiple regression model for compressive strength prediction of high: performance concrete. *J Appl Sci* 2009;9:155–60. <https://doi.org/10.3923/jas.2009.155.160>.
- [41] Naeem M, Bali M, Naeem MR, Amiri JV. Prediction of lateral confinement coefficient in reinforced concrete columns using M5' machine learning method. *KSCE J Civ Eng* 2013;17(7):1714–9.
- [42] Mohammed A, Burhan L, Ghafor K, Sarwar W, Mahmood W. Artificial neural network (ANN), M5P-tree, and regression analyses to predict the early age compression strength of concrete modified with DBC-21 and VK-98 polymers. *Neural Comput Appl* 2021;33(13):7851–73. <https://doi.org/10.1007/s00521-020-05525-y>.

- [43] Salih A, Rafiq S, Sihag P, Ghafor K, Mahmood W, Sarwar W. Systematic multiscale models to predict the effect of high-volume fly ash on the maximum compression stress of cement-based mortar at various water/cement ratios and curing times. *Measurement* 2021;171:108819. <https://doi.org/10.1016/j.measurement.2020.108819>.
- [44] Mohammed A, Rafiq S, Sihag P, Mahmood W, Ghafor K, Sarwar W. ANN, M5P-tree model, and nonlinear regression approaches to predict the compression strength of cement-based mortar modified by quicklime at various water/cement ratios and curing times. *Arabian J Geosci* 2020;13(22):1–16. <https://doi.org/10.1007/s12517-020-06199-5>.
- [45] Mohammed A, Rafiq S, Mahmood W, Al-Darkazalir H, Noaman R, Qadir W, et al. Artificial Neural Network and NLR techniques to predict the rheological properties and compression strength of cement past modified with nanoclay. *Ain Shams Eng J* 2021;12(2):1313–28. <https://doi.org/10.1016/j.asej.2020.07.033>.
- [46] Huang H, Xue C, Zhang W, Guo M. Torsion design of CFRP-CFST columns using a data-driven optimization approach. *Eng Struct* 2022;251:113479.
- [47] Guo M, Huang H, Zhang W, Xue C, Huang M. Assessment of RC frame capacity subjected to a loss of corner column. *J Struct Eng* 2022;148(9):04022122.
- [48] Parsajoo M, Armaghani DJ, Asteris PG. A precise neuro-fuzzy model enhanced by artificial bee colony techniques for assessment of rock brittleness index. *Neural Comput & Applic* 2022;34(4):3263–81.
- [49] Asteris PG, Lourenço PB, Roussis PC, Elpida Adami C, Armaghani DJ, Cavalieri L, et al. Revealing the nature of metakaolin-based concrete materials using artificial intelligence techniques. *Constr Build Mater* 2022;322:126500.
- [50] Asteris PG, Lemonis ME, Le T-T, Tsavdaridis KD. Evaluation of the ultimate eccentric load of rectangular CFSTs using advanced neural network modeling. *Eng Struct* 2021;248(2021):113297. <https://doi.org/10.1016/j.engstruct.2021.113297>.
- [51] Asteris PG, Lourenço PB, Hajihassani M, Adami C-E, Lemonis ME, Skentou AD, et al. Soft computing-based models for the prediction of masonry compressive strength. *Eng Struct* 2021;248:113276.